Tatzel, M., von Blanckenburg, F., Oelze, M., Schuessler, J. A., Bohrmann, G. (2015): The silicon isotope record of early silica diagenesis. - *Earth and Planetary Science Letters*, *428*, pp. 293—303.

DOI: http://doi.org/10.1016/j.epsl.2015.07.018

The silicon isotope record of early silica diagenesis

Michael Tatzel [ab], Friedhelm von Blanckenburg [ab], Marcus Oelze [ab], Jan A. Schuessler [a], Gerhard Bohrmann [c]

[a] German Research Center for Geosciences, GFZ Potsdam, Germany

[b] Department of Earth Sciences, Institute of Geological Sciences, Freie Universität Berlin, Germany

[c] MARUM – Center for Marine Environmental Sciences, Department of Geosciences, University of Bremen, Klagenfurter Str., 28359 Bremen, Germany

Please cite this article as:

Michael Tatzel, Friedhelm von Blanckenburg, Marcus Oelze, Jan A. Schuessler, Gerhard Bohrmann

The silicon isotope record of early silica diagenesis

Earth and Planetary Science Letters 428 (2015) 293–303

Abstract The heavy isotopes of silicon are strongly enriched in some of the youngest, early diagenetically formed porcellanite layers from the Southwest Indian Ridge (Pleistocene) and the Maud Rise (Pliocene). These porcellanite layers are composed of opal-CT and were formed by the conversion of amorphous silica (opal-A) from siliceous sediment via dissolution-reprecipitation. Their bulk δ^{30}Sivalues range between 1.7 and 2.3‰. Detritus-poor siliceous sediment surrounding these layers is significantly lower at -0.3to 1.5‰. Sequential chemical extractions of bulk siliceous sediment show (i) preferential dissolution of diatoms featuring higher δ^{30}Si than radiolaria and Al–Si components. The detailed investigation of porcellanite layers by micro-scale Si isotope and Al/Si analyses using UV femtosecond laser ablation ICP mass spectrometry show that (ii) precipitation of authigenic aluminum silicates enriched in light Si isotopes drives pore waters to even higher δ^{30}Si. We suggest that the same processes redistributed stable silicon isotopes in precursor siliceous sediments of ancient chert. We infer that past environmental conditions can be reconstructed with high fidelity from the stable Si isotope composition of chert when initial seawater Si concentrations were high (such as in the Precambrian). Exchange of Si between layers during phase transformation (from opal-A to opal-CT and from opal-CT to quartz) is impeded when variable amounts of detrital minerals are present, because they control rates of silica phase transformation and hence the timing of dissolution–reprecipitation during burial.

1 Introduction

Today the stable isotopes of silicon are successfully employed to quantify the present and past oceans' environmental conditions and marine biogeochemical cycles. In the modern ocean for example biological silicic acid utilization is inferred from the Si isotope composition of seawater (Cardinal et al., 2005; De La Rocha et al., 1997; Reynolds et al., 2006) or from biogenic silica in diatoms sampled in core top sediments (Egan et al., 2012). This information is crucial for estimating export rates of organic carbon from surface waters and its burial that affects atmospheric carbon dioxide concentrations. In the geologic record the stable Si isotope composition of chert and silicified rocks is used to reconstruct for example the weathering and hydrothermal sources of Si and the distribution of sedimentary Si sinks (e.g. André et al., 2006; Chakrabarti et al., 2012; Fan et al., 2013; Marin-Carbonne et al., 2013, 2012, 2011; Steinhoefel et al., 2010, 2009; van den Boorn et al., 2010, 2007). In spite of this progress we lack an under-standing of whether the measured isotope compositions of sedimentary chert deposits do indeed record primary environmental conditions. This difficulty arises because chert forms by diagenetic dissolution-reprecipitation reactions. The effect of diagenetic overprint on sedimentary Si isotope compositions was testified for example in a study of the Miocene Monterrey Formation. There, Ziegler et al. (2011) found that the stable Si isotope composition (δ^{30}Si) of diagenetic quartz (δ^{30}Si= 0‰) was much lower than that of the amorphous silica in associated diatoms (δ^{30}Si= 1.4‰). The authors attributed this difference to a late diagenetic fluid that had equilibrated with the Monterrey shales. Another result of such dissolution of amorphous precursor silica and reprecipitation of quartz was found in the form of highly variable Si and O isotope compositions measured by micro-scale SIMS analyses of micro-quartz in Precambrian chert, in which δ^{30}Si varied by 2.8‰ on the micrometer scale (Marin-Carbonne et al., 2012). However, such overprinting of isotope compositions is not ubiquitous on the bulk scale. Isotope fractionation was found to be absent during the formation of chert by the silicification of magadiite ($NaSi_7O_{13}(OH)_3 \cdot 3(H_2O)$) (Ziegler and Marin-Carbonne, 2012). Progress in synthesizing these disparate observations into a fundamental understanding of the underlying processes is hampered by our lack of knowledge of the isotope effects associated with diagenetic processes that convert amorphous opal into quartz.

Diagenesis of siliceous sediment means that the abundance of the crystalline SiO_2 polymorphs cristobalite and tridymite (opal-CT) and quartz increases with burial depth at the expense of amorphous silica (opal-A) where time and temperature exert the dominant control over the rate of diagenesis. The slow kinetics of these dissolution–reprecipitation processes explains why most chert deposits found are at least 20 Ma in age (Hesse, 1988). Besides time and temperature, the host sediment's chemical composition exerts a first-order control over rates of diagenesis. Such control is expressed in form of localized porcellanite beds (made up of opal-CT) and chert beds (made up of quartz) in unconsolidated siliceous sediment comprised predominantly of opal-A of the Monterrey Formation (Bramlette, 1946). Porcellanite layers as young as 430ka were found in siliceous sediments of the Southern Ocean (Kerguelen Plateau: Schlich et al., 1989; Weaver and Wise, 1973; Maud Rise: Barker et al., 1988; Bohrmann et al., 1994 and Southwest Indian Ridge (Bohrmann et al., 1994, 1990) and were formed at temperatures of only 0 to 4°C as inferred from their oxygen isotope composition (Botz and Bohrmann, 1991).

The phase transformation from opal-A to opal-CT does not re-quire elevated temperature and can rather be explained by solubility changes of silica polymorphs (Williams et al., 1985). In early marine diagenesis opal-CT forms if the equilibrium solubility of silicon (setting pore water Si concentration with respect to the host sediment) exceeds that of opal-CT (ca. 25 ppm SiO_2 for cristobalite in aqueous solutions at 20°C and standard pressure; (Walther and Helgeson, 1977). At the seawater-sediment interface solutions are dominated by the low seawater Si concentrations (in the modern ocean between 0.6 and 10.8 ppm SiO_2; Tréguer et al., 1995) and are thus strongly undersaturated in Si. With increasing depth, Si concentrations increase gradually and attain equilibrium concentrations asymptotically at about 10 cm sediment depth, i.e. the 'asymptotic pore water concentration' (Van Cappellen and Qiu, 1997a, 1997b). These equilibrium solubilities depend on the composition of the sediment. Pure opal-A has an equilibrium solubility of ca. 60–130 ppm SiO_2 (Williams and Crerar, 1985; Williams et al., 1985). However, this value is significantly modified by pore water pH, the presence of carbonates and Mg-hydroxides in the sediment (Kastner et al., 1977), organic matter (Hinman, 1990), and Na, Mg, K, Al and Fe in solution (Hinman, 1998). Dissolved aluminum, promoted by the dissolution of detrital minerals at the water-sediment interface (van Beusekom et al., 1997), has a particularly strong impact on the solubility of biogenic silica (Dixit et al., 2001). It has been found that the equilibrium solubility of siliceous sediment is reduced by the structural incorporation of Al into opal during biosynthesis (Dixit et al., 2001; Gehlen et al., 2002; van Bennekom et al., 1991) and by the formation of authigenic aluminum silicates (Dixit et al., 2001; Van Cappellen and Qiu, 1997a). Aluminum silicates, i.e., poorly crystalline Al-Si phases containing various amounts of K, Fe, Mg and Cl (Michalopoulos et al., 2000) readily form in the sediment during early diagenesis and can form coatings on biogenic silica, e.g. diatom frustules (Michalopoulos and Aller, 2004; Rickert et al., 2002). In this case the solubility of biogenic silica is reduced and the asymptotic pore water Si concentration is lower than that of the biogenic silica (Hurd, 1973). Thus, during early diagenesis it is the geochemical environment that determines the timing of the phase transformations.

Stable silicon isotope ratios are likely to shift during these phase transformations. In the most simple terms the isotope composition of the pore water Si and the solids precipitated thereof can be affected by i) selective dissolution of silicon sources of variable isotope composition, ii) isotope fractionation during precipitation into solids that differ in their isotope fractionation factor, and iii) the mass balance between dissolution and precipitation. We are now in the position to unravel these effects as recent experimental work has shed light on the isotope fractionation accompanying Si precipitation with unprecedented detail. The precipitation of aluminum silicates is associated with a range of negative isotope fractionation factors ($\alpha^{30}Si_{solid/solution}$) of up to -4.5‰ (Oelze et al., 2015), while the adsorption onto gibbsite is associated with fractionation factors that range between -1.8 and -3.2‰ (Oelze et al., 2014). Both depend on the net solid formation or adsorption rate. In contrast, precipitation of Si from Al-free and low-Al solutions shows that silicon does not fractionate its isotopes upon precipitation, i.e. $\alpha^{30}Si_{solid/solution}$= 0 (Oelze et al., 2015). Furthermore, experimental studies show that preferential precipitation of light silicon isotopes occurs if chemical disequilibrium prevails, and that isotope fractionation is absent at

equilibrium (Geilert et al., 2014; Roerdink et al., 2015). This view is supported by absence of Si isotope fractionation during chert formation (Ziegler et al., 2011).

To evaluate the fidelity of chert as a paleo-environmental archive we explored stable Si isotope fractionation accompanying early marine diagenesis. We sampled the youngest porcellanite found to date. Porcellanites (opal-CT) and the adjacent siliceous sediments (mainly opal-A) were sampled in piston cores from the Southwest Indian Ridge (PS2089-2, Pleistocene) and the Maud Rise (PS2070-1, Pliocene) (Bohrmann et al., 1994). The porcellanite found in these cores was preserved undisturbed in contact with its host sediment. We compared the Si isotope composition of the early diagenetic porcellanite with that of the precursor material. To determine the differential solubility of primary silica sources and to constrain their isotope composition we conducted sequential leaching experiments on bulk, unconsolidated siliceous sediments. To resolve the temporal evolution of opal-CT precipitation the porcellanite layers were investigated in detail by micro-scale silicon isotope analyses using UV femtosecond laser ablation ICP mass spectrometry (fs-LA-MC-ICP-MS). We model the effect that dissolution and precipitation processes have on pore water and porcellanite δ^{30}Si and Al/Si. Finally, we explore the implications for the use of Si isotopes to derive past biogeochemical fluxes from ancient chert.

2 Materials and methods

2.1 Samples

Two cores were recovered with a piston corer during Polarstern cruise ANT-IX/3 at the Southwest Indian Ridge (PS2089-2: Pleistocene; 53°11.3'S, 03°19.7'E; water depth 2618 m) and Maud Rise (PS2070-1: Pliocene; 65°06.3'5, 03°37 'E; water depth 2611 m), respectively (Figure 1). These sediments were deposited during Marine Isotope Stages 11 and 12 (ca. 470 - 360 ka BP: PS2089-2) and be-tween ca. 4.7 and 3.6 Ma (PS2070-1) as deduced from diatom and radiolarian assemblages (Bohrmann et al., 1994). Both cores comprise very pure siliceous ooze, and contain porcellanite layers of a few centimeter thickness. Siliceous sediment was sampled from sediment depths between 7.3 and 5.4 m (PS2089-2), and 6.1 and 4.2 m (PS2070-1), respectively. Each sediment sample represents about one centimeter (Table S.1). We sampled the porcellanite layers that are intercalated with the siliceous ooze at depths of ca. 6.0 m (PS2089-2) and 4.7 m (PS2070-1). The Pliocene porcellanite layer in core PS2070-1 has a wide regional extent and covers large parts of Maud Rise, as inferred from seismic data (Bohrmann et al., 1992).

Sediment from the Pleistocene piston core (PS2089-2) in vicinity of the porcellanite layer has high opal-A contents of up to 90%, is dominated by diatom frustules, and has TOC contents of 0.1 to 0.3% (Bohrmann et al., 1994). Siliceous sediment surrounding the porcellanite layer in PS2070-1 (Pliocene) has opal-A contents of up to 90%, contains variable amounts of mostly diatoms and radiolarians and very minor silicoflagellates, and low TOC contents of <0.05% (Bohrmann et al., 1994).

The grain size ranges from <1µm for shards of broken diatom frustules to ca. 40 µm for undamaged frustules. Radiolarians typically range in size from 50 to 100 µm. Finely dispersed xenomorphic particles are found in variable abundance and constitute detrital as well as authigenic phases (Figure S.1).

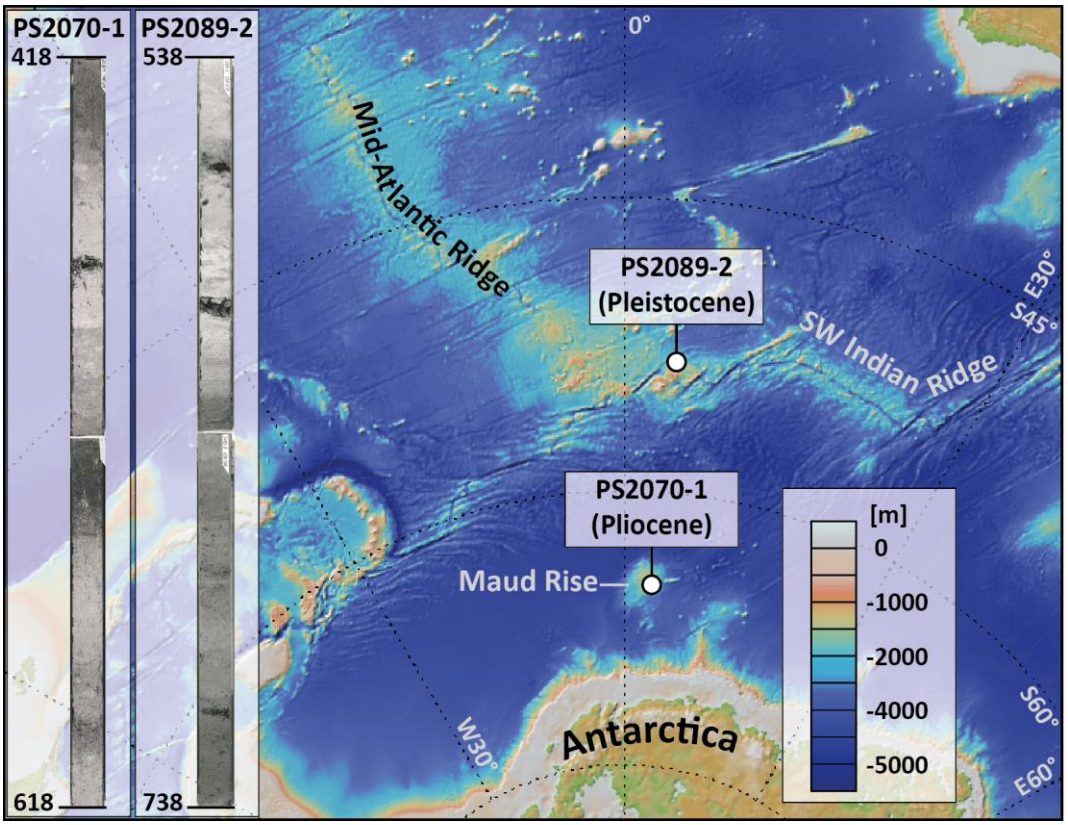

Figure 1: Map (www.geomapapp.com; Ryan et al., 2009) showing the sample locations in the Southern Ocean and photographs of the sampled piston cores (insets). Color coding refers to the depth below sea level

The porcellanite layer from the Pleistocene piston core is comprised of a porous part (sublayer1) characterized by about 5 µm large opal-CT lepispheres that are only in parts intergrown and a dense part (sublayer2) that has little void space (Figure 2a). Opal-CT lepispheres from the Pliocene core cover a size range of <1 µm to ca. 5 µm. The porcellanite layer is irregularly layered and characterized by different coloring that distinguishes the two major sublayers (Figure 2b). In close vicinity to this porcellanite we found an animal burrow of 3.5 to 7 mm thickness and ca. 3.3 cm length that is filled with opal-CT (Figure 2c).

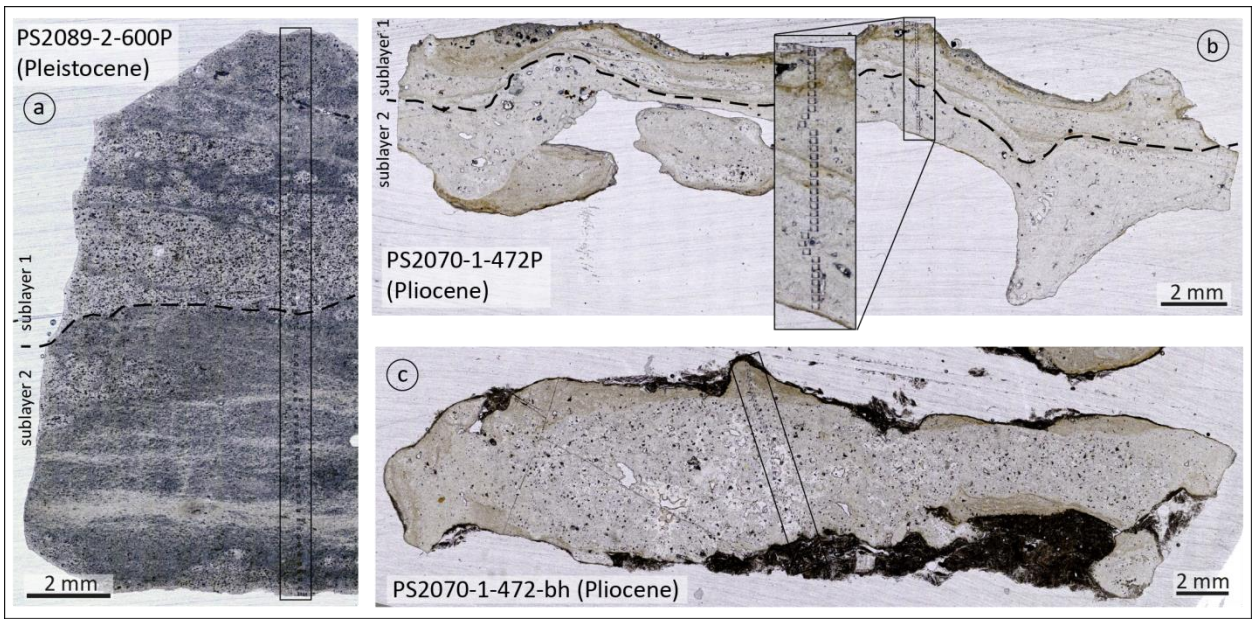

Figure 2: Overview images of thin sections of analyzed porcellanite samples in transmitted light. Frames highlight transects of laser ablation craters from Si isotope analyses (Figure 5). (a) Porcellanites PS2089-2-600P (Pleistocene) and (b) PS2070-1-472P (Pliocene) are comprised of distinct sublayers (separated by dashed lines) and bear variable amounts of impurities as indicated by their color. The inset shows a blow-up of laser craters. (c) Sample PS2070-472-bh is a cut through an animal burrow filled with opal-CT preserved in contact with adjacent siliceous ooze. The concentric texture and color variation indicates that impure precipitates have formed first.

2.2 Methods

2.2.1 Leaching experiments

To identify the Si isotope composition and Al/Si mass ratio of the most soluble component, two types of leaching experiments were conducted on three different bulk sediment samples. Conditions of the experiment are summarized in Table S.8. Experiment I was done at 70°C in a pre-cleaned 50 ml PP tube filled with ca. 5.3 mg sediment sample (PS2070-1-423) to which 50 ml 1.6mM NaOH solution were added. Solutions were sampled in 30 min intervals (ca. 0.2–15ml each time) for 5 h after which the concentration of the remaining NaOH solution was increased to 1M. Another two solution samples were taken after 6.5 and 22.5 h. When Si amounts were too low for individual Si isotope analyses, samples of individual leach steps were combined (Table S.9). In experiments IIa and IIb, 12 splits of each 2.6 to 3.0 mg sediment of PS2070-1-493 (experiment IIa) and PS2089-2-639 (experiment IIb), respectively, were leached separately at room temperature in 25 ml 1.6 mM NaOH in separate pre-cleaned 50 ml PP tubes on a roller mixer. The supernatant solution of each individual tube was sampled after leach durations of 0.5, 1, 1.5, 2, 2.5, 3, 3.5, 4, 5, 6, 8 and 22.5 h and centrifugation. One sample for both experiments, IIa and IIb, was heated to 70°C for 24 h, where sediment was leached with 1.6 mM NaOH in a Teflon beaker on a hotplate. Solutions were prepared for analyses of Si and Al concentrations and for Si isotopes. Selected remaining sediments were recovered for SEM analyses (Figure S.1). Previous studies noted a degradation of the PP tubes by 5 mM NaOH and formation of a white gelatinous-seeming precipitate (Baah and Baah, 2002; Brzezinski and Nelson, 1995). We did not observe such precipitates during the entire leaching procedure.

2.2.2 Sample digestion and Si purification

Samples were prepared for Si isotope analyses using the method of (Georg et al., 2006) with slight modifications. Approximately 15 mg of pulverized, homogenized sediment sample were digested for 15min at 750◦C in a muffle furnace by NaOH fusion (400 mg NaOH pellets, Merck, p.a. grade) in Ag-crucibles. After the dissolution of the fusion cake in Milli-Q water (>18 MΩ) and 1.5mM HCl (pH 1.5), the sample solution was diluted to <30 ppm SiO_2 and acidified to pH 1.5 with HCl. An aliquot of about 50 µg Si of this solution was loaded onto a column (DOWEX AG 50W-X8, 200–400 mesh) from which silicon was eluted with 5 ml Milli-Q water. Solutions sampled during leaching experiments were processed with the same procedure, but silicon amounts were as low as 5µgin some samples. Samples were analyzed by ICP-OES (Varian 720-ES with an uncertainty of about 5%) before isotope analyses to check for column recovery which amounted to >92% Si in all cases, and for purity of the Si sample solution (>95% Si). The fusion/dissolution procedure blank contributed to <0.1% of total Si, and the blank of the Si column procedure was <50ng Si. Element concentrations were determined on diluted sample aliquots after solid sample digestions (as described above) using an axial ICP-OES (Varian 720-ES). See Supplement S1.3 for details.

2.2.3 Solution MC-ICP-MS silicon isotope analyses

Isotope ratios were determined in medium or high resolution mode on a Thermo Neptune multi-collector inductively coupled plasma mass spectrometer (MC-ICP-MS) equipped with a Neptune Plus Jet Interface (using a Pfeiffer OnToolBooster interface pump; Jet sample and H skimmer cones, Apex desolvating nebulizer). Details of the method are described in Supplement S1.1. We report the $^{29}Si/^{28}Si$ and $^{30}Si/^{28}Si$ isotope ratios in the delta notation as per mill deviation ($\delta\times10^3$) from the international reference material NBS-28:

$$\delta^{(x/28)}Si = \left[\frac{\left(\frac{xSi}{28Si}\right)_{sample}}{\left(\frac{xSi}{28Si}\right)_{NBS28}} - 1\right] \quad \text{(Eq. 1)}$$

where x denotes either ^{29}Si or ^{30}Si.

We report average $\delta^{30/28}Si$ values, abbreviated as $\delta^{30}Si$ obtained from 1 to 6 replicate measurements of the same analyte solution together with their 95% confidence interval (= t · SD/√n), which indicates the instrument repeatability (Tables S.1 and S.6). Based on evaluation of accuracy and precision of the sample repeat measurements and comparison of results obtained on reference materials with published data compiled in Jochum et al. (2005; Table S.6), the uncertainty of the entire solution MC-ICP-MS method is estimated to be ±0.07‰ (2SD) for $\delta^{29}Si$ and ±0.10‰ (2SD) for $\delta^{30}Si$ (see Supplement for details). The same estimate was obtained by statistical evaluation according to equation (2) in Schoenberg and von Blanckenburg (2005), based on repeat analyses of all samples analyzed in this study. This uncertainty is used for data interpretation in this study.

2.2.4 Femtosecond LA-MC-ICP-MS analyses

The micro-scale silicon isotope composition and Al/Si ratios were determined on three samples (PS2089-2-600P, Pleistocene; PS2070-1-472P, Pliocene and PS2070-1-472-bh, Pliocene) of porcellanite (opal-CT) by UV femtosecond laser ablation MC-ICP-MS (UV fs LA-MC-ICP-MS, Fem2) at GFZ Potsdam. Instrumentation and analytical conditions are described in Supplement S.1.2 and in Schuessler and von Blanckenburg, (2014). Laser ablation was performed along transects across porcellanite layers with a spatial resolution at each analysis location of about 100 ×100 µm surface area with less than 10 µm crater depth. We report results in the δ-notation as per mil deviation relative to NBS-28 together with the internal standard error of the mean (2SE at 95% confidence) of single sample measurements (Tables S.3, S.4, S.5), which is typically <0.1‰ for δ^{30}Si as calculated by error propagation from measurements of one sample and the two bracketing NBS-28 standards. The uncertainty of the fs LA-MC-ICP-MS method (external longterm repeatability) is ±0.15‰ (2SD) for δ^{29}Si and ±0.23‰ (2SD) for δ^{30}Si, respectively (Schuessler and von Blanckenburg, 2014). These uncertainties should be applied for geological interpretation and comparison to results obtained by other laboratories. In this study, accuracy was verified by repeat measurements on reference materials during each analytical session (Table S.7).

3 Results

3.1 Bulk sample Si isotope and Al/Si ratios

SiO_2 concentrations of siliceous sediment in the Pleistocene core range from 52 to 76 wt% and from 68 to 76 wt% in the Pliocene core. Porcellanites contain 87 to 92 wt% SiO_2. Other major element concentrations of bulk sediment samples are reported in Table S.5. and comprise mainly Al, Fe, Mg and Ca. In the vicinity of the porcellanite layers, the concentration of all measured cations is lower than in the surrounding sediments. Al/Si ratios are shown as indicator for detrital minerals and are low in porcellanite layers and adjacent siliceous sediment layers (Figure 3).

In samples from the Pleistocene core between 730 and 541 cm sediment depth, bulk sediment δ^{30}Si ranges from 0.16 to 1.50‰. The dense part of the porcellanite (sublayer 2, Figure 2a) has a bulk δ^{30}Si of 1.96‰ (n= 3; Table S.1, Figure 3). In the more porous part (sublayer 1, Figure 2a) δ^{30}Si is at 1.69‰. In the Pliocene core bulk sediment samples from depths between 613 and 423 cm range between -0.34 and 0.61‰. The bulk analysis of the Pliocene porcellanite layer (PS2070-1-472P) yielded δ^{30}Si of 2.28‰.

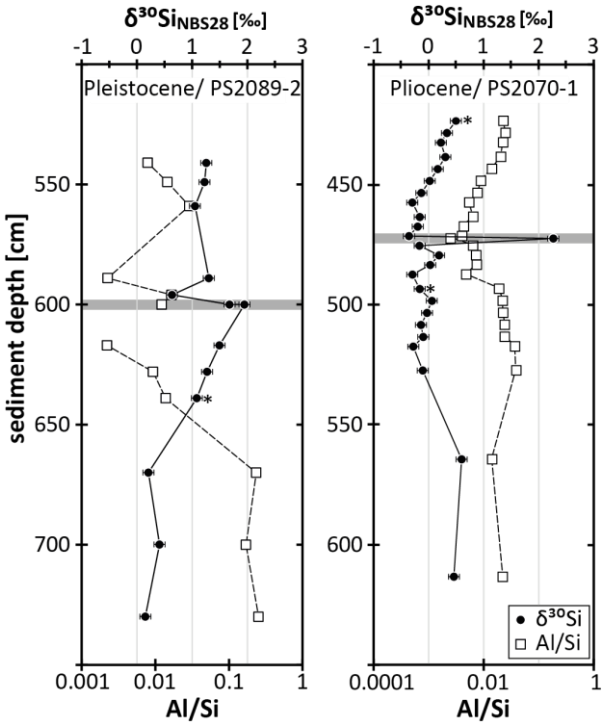

Figure 3: Bulk sediment δ^{30}Si (solid circles) and Al/Si mass ratios (open squares) in Pleistocene (PS2089-2) and Pliocene (PS2070-1) siliceous sediments and porcellanite (indicated by horizontal gray bar). Error bars on δ^{30}Si represent uncertainty of the solution MC-ICP-MS method (±0.10‰, 2SD). Uncertainties on Al/Si mass ratios are smaller than the symbol size. See Tables S.1 and S.5 for data. Samples used in leaching experiments (Figure 4, Tables S.8 and S.9) are indicated by∗.

3.2 Results from leaching experiment

We describe the results of the leaching experiments as measured in the supernatant solutions after separation from the remaining solutions. The silicon concentrations obtained in experiment I (PS2070-1-423) show that the fraction of Si dissolved during the extractions increased from ca. 0.6 to 68% of the total initial solids Si with increasing run duration (Figure 4). The δ^{30}Si values and Al/Si ratios in the solutions are generally higher than the bulk sediment, with the exception of two samples that were extracted after switching from 1.6 mM to 1M NaOH. In experiment IIa (PS2070-1-493) 1.5 to 43 wt% of the total silicon was dissolved. Solutions yielded δ^{30}Si values from 0.55 to 1.08‰, which is considerably heavier than the bulk sediment (-0.15‰). Al/Si ratios are systematically higher than that of the bulk sediment.

In experiment IIb (PS2089-2-639; Pleistocene) between ca. 1.4 and 27 wt% of the initial solid silicon was dissolved. In contrast to the other experiments, the solutions' δ^{30}Si evolved from 0.28 to 1.00‰ and is thus systematically lower than the bulk sediment sample (1.09‰). As in leaching experiments I and IIa, Al/Si ratios in the solutions sampled in 1.6 mM NaOH are higher than Al/Si in the bulk sediment.

Common to all leaching experiments is that Si in the first sampled solutions is lower in δ^{30}Si than that sampled at a later point in time (Figure 4). This observation is made regardless of whether the sediment samples are comprised of both diatoms and radiolarians (experiments I and IIa) or mainly

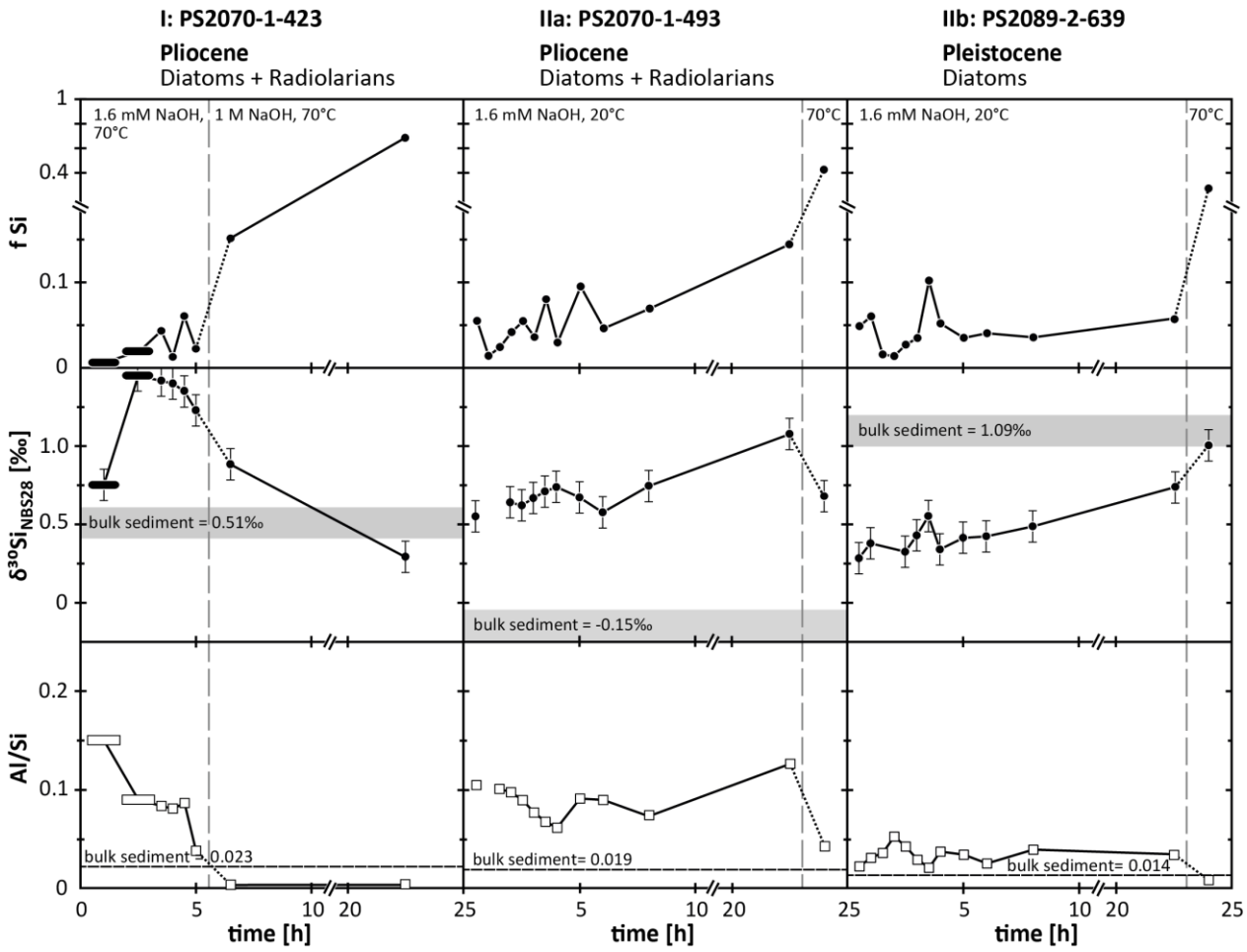

Figure 4: Results from leaching experiments showing relative amounts of dissolved silicon, expressed as fraction Si dissolved relative to the total Si in the sediment (f Si), δ^{30}Si of dissolved Si and Al/Si mass ratios in leachates for both experiments I (sequential extractions) and IIa +IIb (batch extractions). Samples PS2070-1-423 and 493 (Pliocene) contain mostly diatoms and radiolarians and PS2089-2-639 (Pleistocene) contains mostly diatoms. Error bars on δ30Sirepresent uncertainty of the solution MC-ICP-MS method (±0.10, 2SD). Horizontal gray lines indicate the bulk sediment Al/Si mass ratio and δ^{30}Si. Vertical dashed lines indicate the time at which experimental conditions were switched with respect to NaOH molarity or temperature

diatoms (experiment IIb). These first solutions are also characterized by Al/Si ratios greater than that of their respective bulk sediment, suggesting that aluminum silicates are dominating the first leaching steps. This observation is supported by SEM analyses and EDS spectra reported in Rickert et al., (2002) and Michalopoulos et al. (2000), who report aluminum silicate formation on diatom opal. SEM images (Figure S.1) of PS2070-1-493 show that radiolarians are dominating the residual sediment after leaching experiment I. Therefore radiolarians are less soluble and appear to contain Si that is lower in δ^{30}Si than diatoms as indicated by higher δ^{30}Si in experiment IIa. Low δ^{30}Si and high Al/Si ratios in experiment IIb (mostly diatoms) reveal that the first dissolving components are aluminum silicates that have likely formed from early diagenetic solutions. Only when a high mass fraction of the sediment (here 27 wt%) is dissolved, the δ^{30}Si of the leachate approaches that of the bulk sediment, which is mainly comprised of diatoms. Consequently, diatoms and covering early diagenetic aluminum silicates preferentially dissolved in all leaching experiments. Owing to the dominance of diatoms, the Pleistocene sample (PS2089-2-639) reveals no apparent differences in its composition following the treatment (Figure S.1).

3.3 Results from micro-scale Si isotope analyses

δ^{30}Si from micro-scale Si isotope analyses are in good agreement with those from bulk analyses by solution ICP-MS. Analyses of silicon isotope ratios and the Al concentration on a thin section across porcellanite sample PS2089-2-600P (Pleistocene) yielded δ^{30}Si between 1.21 and 2.07‰ and Al concentrations from 447 to 3843 ppm (Table S.2). Opposing trends of Al/Si and δ^{30}Si characterize this porcellanite layer. A pronounced drop in δ^{30}Si matches increased Al concentrations and occurs at the interface of two distinct sublayers (Figure 5a and Figure 2a).

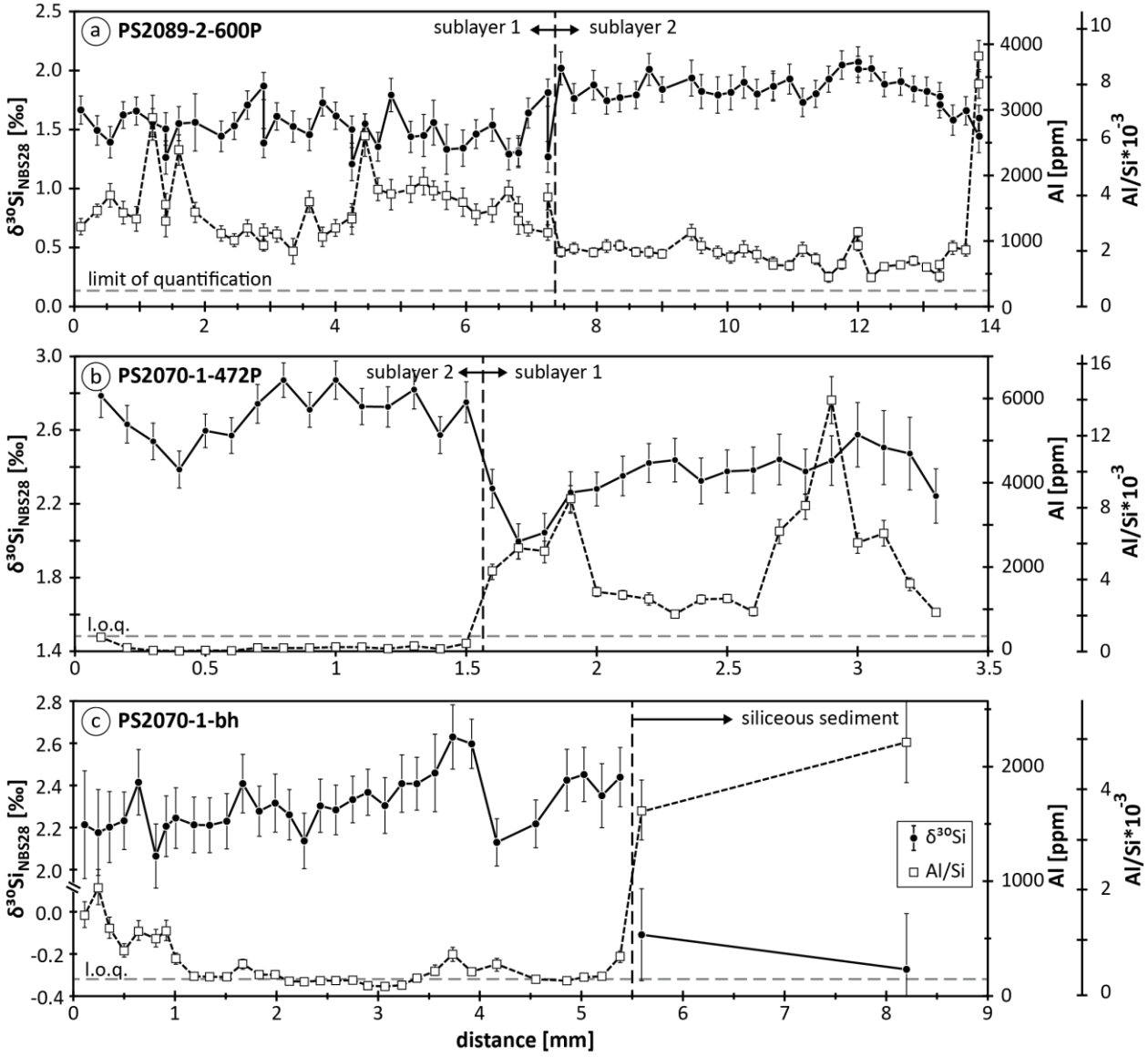

Figure 5: Micro-scale silicon isotope ratios (black circles), Al/Si mass ratios and derived Al concentrations [ppm] (open squares) on transects across porcellanite layers by femtosecond laser ablation MC-ICP-MS analysis from (a) Pleistocene (PS2089-2-600P; Table S.2), and (b) Pliocene (PS2070-1-472P; Table S.3) porcellanite layers as well as (c) the opal-CT filled animal burrow (PS2070-1-472-bh; Table S.4). The vertical dashed line delineates sublayers of the porcellanite (a, b; cf. Figure 2) and the contact to the surrounding siliceous sediment (c). The horizontal dashed line represents the lower limit of quantification for Al concentration measurements. Error bars represent the internal standard error of mean values (2SE for n ≈80 integrations at 1s).

In PS2070-1-472P δ^{30}Si ranges from 2.12 to 2.95‰ and Al concentrations vary between 878 and 5931 ppm where for some analyses Al concentrations were below limits of quantification (<350 ppm) (Table S.3). At the interface of two distinct sublayers there is a significant increase in Al concentrations which coincides with a drop in δ^{30}Si (Figure 5b and Figure 2b). We regard the sections in which δ^{30}Si and Al/Si correlate to denote simultaneous precipitation of opal-CT and authigenic Al-silicates. Layers featuring Al concentrations >2000 ppm and no correlation of δ^{30}Si and Al/Si are possibly due to the presence of Al-bearing phases.

Within an opal-CT filled, tube-shaped animal burrow (PS2070-1-472-bh) δ^{30}Si ranges from 2.06 to 2.63‰ (Table S.4). Al concentrations range between 145 and 910 ppm, where for some analyses Al concentrations were below limits of quantification (<130 ppm) and are elevated towards the rims, where also δ^{30}Si values are lower (Figure 5c). Two analyses of adjacent siliceous sediments yield δ^{30}Si of -0.11 and -0.27‰ and Al concentrations of 1580 and 2181 ppm. Micro-scale Si isotope analyses show an internal variability of less than 0.3‰ in δ^{30}Si within porcellanite layers of both cores and reveal a systematic negative correlation of Al concentrations with the isotope composition of silicon.

4 Discussion

4.1 Processes setting the Si isotope ratios and Al/Si in early diagenetic porcellanite

The unique features of our studied cores are 1) that they contain some of the youngest porcellanites found to date, 2) that these porcellanites are isotopically heavier than the bulk surrounding sediments, and 3) that δ30Si in porcellanite increases with decreasing Al/Si (Figure 6). Unraveling the processes underlying these observations are key to understanding the behavior of Si isotopes during diagenesis in general.

Regarding 1), early diagenetic porcellanite is rare and forms apparently exclusively in very pure siliceous oozes (Bohrmann et al., 1994; Murata and Nakata, 1974). It forms from solutions in which the SiO_2 concentrations exceed ca. 25 ppm, i.e. the solubility of cristobalite at 20°C (Walther and Helgeson, 1977) which is the estimated minimum equilibrium solubility of opal-CT (Williams et al., 1985). This condition is rarely found in siliceous deep-sea sediments that typically contain significant abundances of detrital minerals. The presence of detrital minerals reduces the pore water Si concentrations that will therefore remain below the opal-CT equilibrium solubility.

Finding 2), the enrichment of ^{30}Si in porcellanite, can be explained in different ways: (i) isotope fractionation partitioning preferentially heavy Si isotopes into solution during incipient stages of dissolution of opal-A particles; (ii) heavy isotopes are enriched in opal-CT during precipitation ($\alpha > 1$); (iii) the solubilized component from sediment comprising multiple components with different solubilities and isotope compositions is isotopically heavy; (iv) light silicon isotopes are removed from solution by precipitation prior to precipitation of opal-CT.

With respect to explanation (i), isotope fractionation during dissolution of biogenic silica particles, only the preferential release of light isotopes due to kinetic isotope fractionation was reported for basalt and phytoliths (Ziegler et al., 2005), pedogenic clay minerals (Cornelis et al., 2014), and diatoms (Demarest et al., 2009). However, Wetzel et al., (2014) showed the absence of Si isotope fractionation during dissolution of diatom silica. Our leaching experiment IIb supports their observation. Even though release of light Si isotopes is observed in the early phase of dissolution, we interpret the preferential release of light Si to show the light Si isotope composition of the first dissolving aluminum silicates. (ii) Enrichment of heavy isotopes ($\alpha > 1$) during silica precipitation in low temperature environments has not been observed to date and is thus considered unlikely. Rather, secondary silica precipitation typically enriches the solid in ^{28}Si (Basile-Doelsch et al., 2005; Cornelis et al., 2014; Geilert et al., 2014; Roerdink et al., 2015; Ziegler et al., 2005) where isotope fractionation during precipitation depends on the net solid formation rate and can also occur with $\alpha = 1$ (e.g., Oelze et al., 2015, 2014). We therefore regard (iii) preferential dissolution of isotopically distinct sediment components as a first likely explanation. In siliceous sediment that comprises both radiolarians and diatoms, diatoms are expected to dissolve at higher rates. This expectation is indicated from relative enrichment of radiolarians over diatoms in sediment traps and on the seafloor (Abelmann and Gersonde, 1991). Also, the $\delta^{30}Si$ of radiolarians is considerably lower than that of diatoms as demonstrated by Egan et al. (2012). This is for two main reasons: 1) The fractionation factor of silicon isotopes is biologically controlled and varies between different Si-secreting organisms. For example, $\alpha^{30}Si_{diatom\text{-}water}$ is species dependent and varies between -0.5 and -2.1 (Sutton et al., 2013). 2) Diatoms exclusively dwell in the photic zone where intensive silicon utilization induces high surface water $\delta^{30}Si$. In contrast, radiolarians dwell at all water depths and thus take up silicon from water masses that are enriched in light silicon isotopes relative to surface waters through the dissolution of sinking biogenic silica (Ehlert et al., 2012; Reynolds et al., 2006). Consequently, diatoms will commonly be heavier in $\delta^{30}Si$ than radiolarians. Our leaching experiments support this prediction. The Pliocene piston core shows increased modal abundances of radiolarians after the leaching experiment (Figure S.1), suggesting that diatoms are more soluble than radiolarians. The decrease in the solutions' $\delta^{30}Si$ in the later stages of the leaching sequence (Figure 4, experiments I, IIa) is due to the increasing proportion from silicon of dissolving radiolarians, suggesting that diatoms are enriched in ^{30}Si relative to radiolarians.

Explanation (iv), the initial removal of light silicon isotopes by precipitation of aluminum silicates enriched in light Si isotopes that shifts the pore water $\delta^{30}Si$ to higher values, is the second likely cause for the isotopically heavy Si in porcellanite. The latter explanation also explains finding 3), that $\delta^{30}Si$ in porcellanite increases with decreasing Al/Si (Figure 6). We note that during simultaneous sedimentation and early diagenesis these processes will not proceed in a steady manner: they will shift with changing composition of the deposited sediment, and hence with sediment depth and time. We proceed to explore the evolution of pore water in a simple box model (Figure 7) to scrutinize whether the measured $\delta^{30}Si$ vs. Al/Si trend in porcellanite layers follows vectors in $\delta^{30}Si$ vs. Al/Si space predicted by a mass balance model.

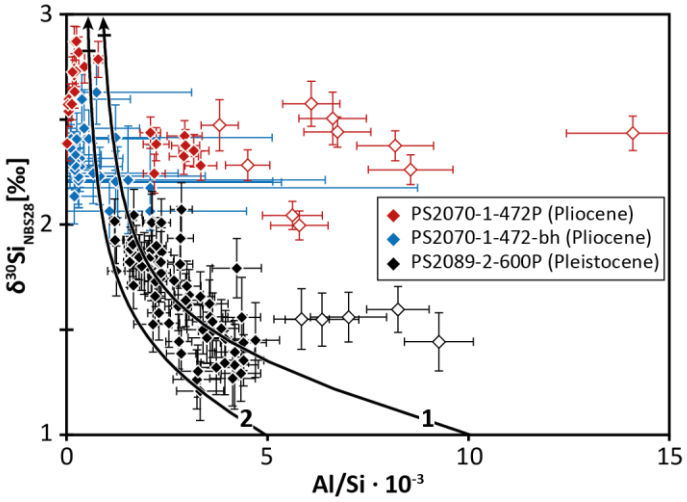

Figure 6: The shift of porcellanite δ^{30}Si with Al/Si mass ratio (solid symbols). Open symbols represent outliers in which laser ablation analyses were likely affected by the presence of detrital Al-rich phases contained within porcellanite (see Section 3.3). The overall negative trend is suggested to present pore water evolution driven by ongoing precipitation of aluminum silicates enriched in isotopically light Si that shifts the residual pore water towards higher δ^{30}Sivalues. Two trends of pore water evolution were modeled based on equations (2) and (3) and the assumptions reported in Section4.2.

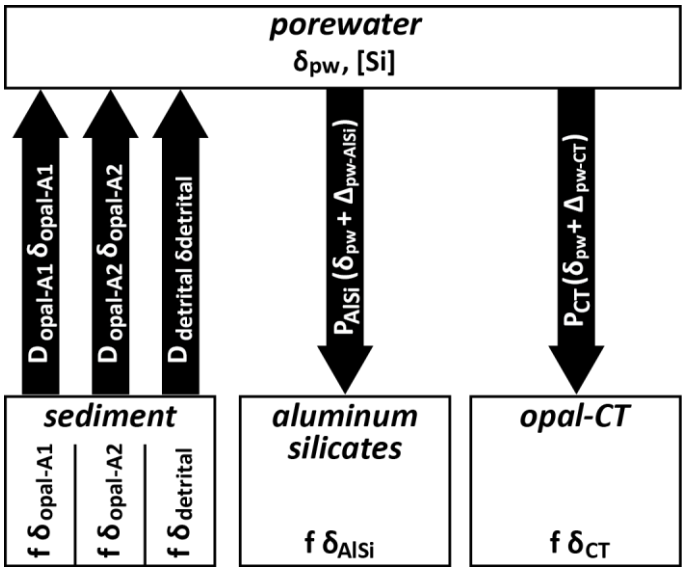

Figure 7: Simple box model showing the principal components involved in early diagenesis of silica. The relative mass fraction of each component is *f*, their isotope composition δ. Dissolution fluxes are represented by *D*, precipitation fluxes by *P*. Δ are the Si isotope fractionation factors for silica precipitation. [Si] is the silicon concentration in pore water. In the present case opal-A1 and opal-A2 are represented by diatoms and radiolarians, respectively. Equation (2) describes this box model.

4.2 Si mass fluxes and isotope fractionation during early diagenesis

The mass fluxes and associated Si isotope fractionation when pore waters exchange with sedimentary compartments during selective opal dissolution, and simultaneous aluminum silicate- and opal-CT precipitation during early diagenesis are shown in Figure 7. The pore water mass balance can be quantified by a differential equation that describes the change in the mass of dissolved pore water Si and its isotope composition:

$$\frac{d}{dt}\left(M_{pw}\delta_{pw}\right) = D_{opal-A1}\,\delta_{opalA1} + D_{opal-A2}\,\delta_{opalA2} + D_{detrital}\,\delta_{detrital} - P_{AlSi}\left(\delta_{pw} + \Delta_{pw-AlSi}\right) - P_{CT}\left(\delta_{pw} + \Delta_{pw-CT}\right) \quad \text{(Eq.2)}$$

where M_{pw}[mass] is the mass of dissolved silicon in pore water (pw) and δ_{pw} [‰] its isotope composition; $D_{opal\text{-}A1}$ [mass/time] is the dissolution flux of opal-A component 1 with an isotope composition $\delta_{opal\text{-}A1}$ [‰]; D_{opalA2}[mass/time], $\delta_{opal\text{-}A2}$ [‰] and $D_{detrital}$ [mass/time], $\delta_{detrital}$ [‰] are the dissolution fluxes and isotope compositions of opal-A component 2 and detrital minerals, respectively; P_{AlSi} [mass/time] is the precipitation flux between pore water and precipitated aluminum silicates; $\Delta^{30}Si_{AlSi\text{-}pw}$ [‰] the isotope fractionation factor between pore water and aluminum silicates; P_{CT}[mass/time] is the precipitation flux from pore water into opal-CT; and $\Delta^{30}Si_{CT\text{-}pw}$ [‰] is the isotope fractionation factor between pore water and opal-CT. Aluminum silicate precipitation from pore water will shift its Al/Si ratio. Equation (2) can be recast accordingly for Al/Si ratios:

$$\frac{d}{dt}\left(M_{pw}Al/Si_{pw}\right) = D_{opal-A1}\,(Al/Si)_{opal-A1} + D_{opal-A2}\,(Al/Si)_{opal-A2} + D_{detrital}\,(Al/Si)_{detrital} - P_{AlSi}\left((Al/Si)_{pw}\cdot K_{pw/AlSi}\right) - P_{CT}\left((Al/Si)_{pw}\cdot K_{pw/CT}\right) \quad \text{(Eq.3)}$$

where $K_{pw/AlSi}$ and $K_{pw/CT}$ [(mass/mass)/(mass/mass)] are elemental fractionation factors for aluminum silicate and opal-CT precipitation from pore water, respectively. The time dependence in both equations arises through continuous sedimentation over depth *z*, where *dt*= (*dz*/sedimentation rate). We assign fractional dissolution fluxes to the different source components. We model the approach to steady state by first-order rate constants describing P_{AlSi} and P_{CT} as a function of the pore solutions' inventories.

We model two scenarios where 1) represents possible conditions for the Pleistocene porcellanite (PS2089-2) and 2) for Pliocene porcellanite (PS2070-1). For 1) we assume almost exclusive diatom dissolution ($D_{opal\text{-}A1}$contributes 99.5%) because this sediment is comprised almost entirely of diatoms. Their isotope composition we constrain from bulk sediment to be δ^{30}Si= 1.5‰ (Section 3.2). The detrital mineral dissolution flux $D_{detrital}$ was assumed to contribute 0.5% and was assigned δ^{30}Si= -0.5‰ as commonly measured in clay. For 2) we assume dominant diatom dissolution with $D_{opal\text{-}A1}$contributing 89% with δ^{30}Si= 1.7‰, as estimated from leaching experiments (Section 3.2). Detrital mineral dissolution was assumed to contribute 1% with δ^{30}Si= -0.5‰. Because the Pliocene core also features radiolarians we assume that these contribute a flux $D_{opal\text{-}A2}$ of 10%. Their δ^{30}Si must be negative as shown by leaching experiments (Section 3.2); here we use δ^{30}Si= -1‰. For simplicity, in both scenarios we assume $(Al/Si)_{opalA1}$= 0, $(Al/Si)_{opalA2}$= 0, $(Al/Si)_{detrital}$= 0.5, which is typical for clays. We assume that opal-CT

precipitation has a negligible leverage to shift pore water Al/Si ratio which is governed to a large extent by $D_{detrital}$ and P_{AlSi}; hence we set PCT to be zero. A test of this assumption is possible if the sequence of precipitation of opal-CT can be reconstructed. Fortunately, such a sequence is preserved in the form of an opal-CT filled burrow (Figure 2c), which reveals elevated Al-concentrations at the upper rim (where precipitation occurred first) and virtually Al-free opal-CT in its center. This finding indicates that opal-CT precipitation did not affect the opal-CT Al/Si because the ratio would otherwise increase during precipitation, i.e. towards the center of the burrow. Thus, silicon is precipitated in preference to aluminum and we therefore assume that $(Al/Si)_{pw}$ is changing only by the precipitation of aluminum silicates.

The silicon isotope fractionation factor $\Delta_{pw\text{-}AlSi}$ is assumed in both scenarios to be = -2‰, in agreement with estimates from Oelze et al. (2015, 2014). We assume the initial pore water compositions to represent those of deep seawater (i.e. $\delta^{30}Si$= 1‰, $[SiO_2]$= 2.2ppm; De La Rocha et al., 2000). We estimate $K_{pw/AlSi}$ from the highest $(Al/Si)_{CT}$ measured in porcellanite which are 0.005 (scenario 2) and 0.01 (scenario 1) and measured $(Al/Si)_{pw}$ in pore water of Southern Ocean cores which is between ca. 0.00015 and 0.0015 (van Beusekom et al., 1997). For the two scenarios specific $K_{pw/Al}$ were found by fitting to be 4 and 10 for the two scenarios. We note that while we model pore water $\delta^{30}Si$ and Al/Si, our data is obtained on porcellanite (Figure 6). Our porcellanites' temporal evolution nevertheless records pore water $\delta^{30}Si$ because during pure opal-CT precipitation $\Delta_{pw\text{-}CT}$ is likely zero (Oelze et al., 2015; Roerdink et al., 2015). As the initial $(Al/Si)_{pw}$ is not known we evaluate relative trends in $(Al/Si)_{CT}$ instead, and assume that these reflect relative trends in $(Al/Si)_{pw}$.

The dominant processes that control pore water $\delta^{30}Si$ and hence $\delta^{30}Si$ of opal-CT are selective dissolution of isotopically heavy diatom silica and ongoing precipitation of isotopically light aluminum silicates. Trends explored by the model are compatible with the microscale $\delta^{30}Si$ and Al/Si record (Figure 5 and Figure 6) where within porcellanite layers, the Si isotope composition co-varies with Al/Si ratios (Figure 6).

4.3 How early diagenetic opal-CT forms

Whether early diagenetic opal-CT can form is dominantly controlled by the detritus content of siliceous sediments. The detritus content determines early diagenetic reactions that control the equilibrium solubility of the bulk sediment (Dixit et al., 2001). Detritus-poor sediments can be formed under conditions of high opal sedimentation rates (e.g., diatom blooms) (Ragueneau et al., 2000) that dilute simultaneously deposited detritus. Upon shallow burial, the dissolution of opal-A in silicon-undersaturated pore water successively increases the pore water silicon concentration until the asymptotic pore water concentration is attained (Figure 8a). Depending on the detrital content, the solubility of opal-CT will be exceeded (Figure 8a, c) and early diagenetic opal-CT will begin to form a few centimeters beneath the sea floor. Over the same depth interval, leachable detrital minerals partially dissolve and authigenic aluminum silicate minerals will form as suggested by pore water Al/Si (Figure 8b).

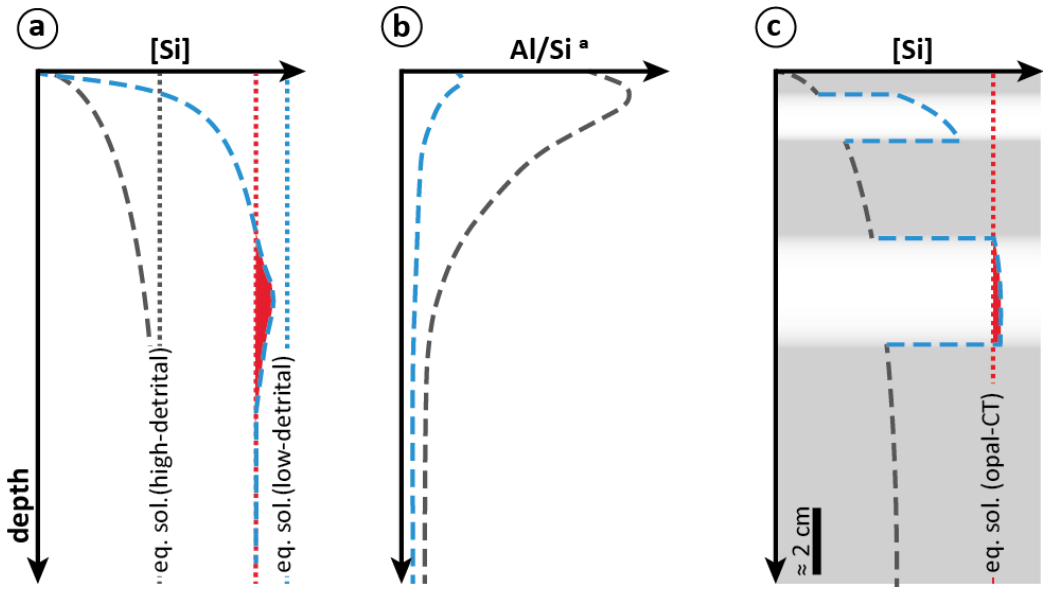

Figure 8: Conceptual model of early diagenetic porcellanite formation in siliceous sediment. Shown are (a) pore water silicon concentration depth profiles for high-detrital (gray) and low-detrital (blue) siliceous sediment. Their corresponding Si equilibrium solubilities are shown with dotted lines in the same color. The equilibrium solubility of opal-CT is shown as a red dotted line and sites of opal-CT precipitation are shown as a red shade. (b) Pore water Al/Si ratio depth profiles (simplified after Van Cappellen and Qiu, 1997a) for high-detrital (gray) and low-detrital (blue) sediment; (c) a schematic stack of siliceous sediment with variable detritus-contents (gray: high, white: low) and the corresponding pore water silicon concentrations. Early diagenetic opal-CT formation occurs in sections with low detritus-contents.

5 Implications for the use of sedimentary Si isotope records in the reconstructions of past biogeochemical cycles

Finally, we use the processes derived above to draw conclusions on the preservation potential of the sedimentary silicon isotope record in chert. The best preservation is attained if the bulk chert δ^{30}Si will reflect that of the original δ^{30}Si of the sediment once deposited. The preservation potential depends on a) depositional conditions including the Si concentration in sea water, the sedimentation rate, and the detrital mineral content, as well as on b) properties of the deposited silica including the number of sedimentary silica components, their isotopic difference, and their difference in susceptibility to dissolution.

5.1 Bulk sediment δ^{30}Si modification during early silica diagenesis

The strongest control on the preservation of the original δ^{30}Si in bulk chert appears to be the sea water silicon concentration. Sea water Si concentrations decreased over the Phanerozoic through the ecological success of radiolarians and sponges in the Paleozoic and diatoms in the Jurassic (Kidder and Erwin, 2001). We therefore expect that the potential to preserve the original δ^{30}Si in bulk chert decreases through geological time, and with it, the record of past biogeochemical cycles.

Chert that formed from sediment deposited in environments with low dissolved Si concentrations will commonly not record the original bulk sediment δ^{30}Si because of effective recycling of

predominantly labile silica to sea water. Exceptions are conditions where 1) only one silica component was present at sedimentation, 2) the difference in isotope composition between components was negligible, 3) the difference in dissolution susceptibility is negligible, and 4) the fraction of soluble silica is low. Therefore, most Mesozoic and Cenozoic chert that formed from siliceous sediment with more than one silica component and with different isotope compositions and susceptibility to dissolution (most commonly radiolarians and diatoms) will have a bulk δ^{30}Si value that is shifted towards the δ^{30}Si of the less soluble component (Figure 9a). Chert that formed from only one opal component, such as pure diatom ooze, is expected to have shifted only minimally from the sedimentary bulk δ^{30}Si.

Early diagenetic dissolution of silica is inhibited by high dissolved Si. Chert that formed from siliceous sediment deposited in environments characterized by high dissolved Si concentrations have a high potential to preserve the original δ^{30}Si (Figure 9b). Precambrian cherts likely preserve the original δ^{30}Si because sedimentation occurred when sea water was still Si-rich. For example the isotopic fingerprint of the earliest forms of biogenic silica, i.e. that in radiolarians and sponges, is likely preserved in Neoproterozoic to Paleozoic chert.

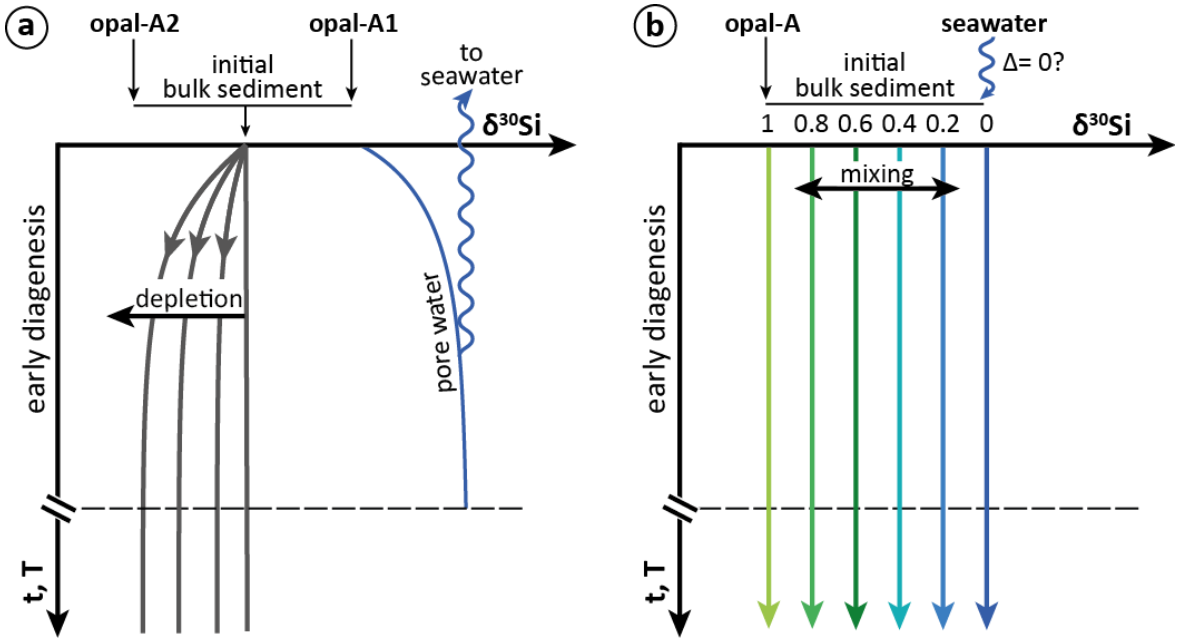

Figure 9: Conceptual presentation of the diagenetic change in Si isotope composition of siliceous sediment under conditions of Si-poor seawater like in the modern ocean (a) and Si-rich seawater like in the Precambrian ocean (b). (a) Sediment consists of two opal components that differ in δ^{30}Si. Pore water is isotopically heavy because the isotopically heavy component (opal-A1) dissolves preferentially and because aluminum silicates enriched in light Si isotopes precipitate. This pore water escapes to seawater. The bulk sediment is depleted in the more soluble component (opal-A1) to a degree that depends on initial mixing proportions of opal-A1 and opal-A2 and their difference in dissolution intensity. No further selective Si isotope loss is expected to occur after early diagenesis (shown beneath the dashed line). (b) Under conditions of high Si concentrations in seawater, the bulk sediment δ^{30}Si will represent a mixture of sedimentary opal-A components that are not selectively dissolved as in scenario (a) due to the high dissolved Si concentrations. During early diagenesis Si precipitated from seawater is added to the opal (the final relative proportions of which are shown by the numbers). The isotope composition of the resulting mixture is preserved during both early and late diagenesis.

5.2 Late diagenetic modification of bulk chert δ^{30}Si during phase transformation

Siliceous sediments will be subject to conversion to opal-CT through increasing temperature during sediment burial. Sedimentary layers will convert to chert at different times and depth that depend on the detrital mineral contents (Isaacs, 1982). We suggest that independently of the timing of opal-CT formation, opal-CT likely carries the δ^{30}Si of the pore water at the moment of supersaturation. Early diagenetically formed opal-CT (from pure siliceous sediment) will record the pore water composition of the most soluble silica whereas later formed opal-CT (from less pure siliceous sediment) will record the isotope composition of less soluble silica that did not dissolve during early diagenesis. Pore water will be locally mobile and hence affect the micro-scale silicon isotope composition. However, on the bulk sediment scale, chemically distinct layers of opal will transform in isolation from each other, precluding isotopic exchange between layers and leaving the bulk (post-early diagenesis) silicon isotope composition likely unaffected. While the oxygen isotope composition of opal-CT and chert is equilibrated at ambient temperatures where dissolution–reprecipitation occurs (Murata et al., 1977), the silicon isotope composition is predicted to be insensitive against isotopic overprinting by such diagenetic fluids because Si concentrations in solution are comparably low. The same considerations hold for the conversion from opal-CT to quartz.

6 Conclusions

Porcellanite layers (made of opal-CT) that form during early diagenesis of siliceous sediment record the Si isotope composition of pore water from which they form. In Si-poor seawater, two fundamental processes affect the isotope composition of both the pore water and the residual siliceous sediment: (i) selective dissolution of (isotopically distinct) sedimentary biogenic silica and (ii) precipitation of authigenic aluminum silicates enriched in light Si isotopes. A corollary is that the pore water isotope composition first is not identical to the bulk sediment (and thus differs from that of opal-CT) and second changes with time during early diagenesis at an extent that is determined by a) the silicon concentration in sea water, b) the sedimentation rate (because it controls the residence time of sediment in the zone of Si undersaturation), and c) the detrital mineral content (because it controls the equilibrium solubility). Sign and magnitude of the offset between bulk sediment δ^{30}Si and pore water δ^{30}Si is furthermore controlled by properties of the deposited opal including d) the number of isotopically different sedimentary opal components, e) their difference in solubility, and f) their relative mass fractions. We infer that opal-CT formed from siliceous sediment deposited in environments with high Si concentrations (such as the Precambrian ocean) will faithfully record paleo-environmental conditions because dissolution is suppressed by high Si levels. We predict that the Si isotope record of opal-CT – regardless of the degree of modification by early silica diagenesis – will be preserved during the late diagenetic conversion to quartz chert.

Acknowledgements

The first author is grateful for funding provided by the DFG through FOR736 "The Precambrian–Cambrian Ecosphere (R)evolution: Insights from Chinese microcontinents" (grant no. BL 562/11-2). We greatly appreciate the support from scientists and technicians of the Alfred-Wegener-Institut, Helmholtz-Zentrum für Polar-und Meeresforschung during the sampling of the cores in the AWI core repository. We thank J. Evers for supporting SEM analyses. Comments by G.F.de Souza, two anonymous reviewers and AE G. Henderson were highly appreciated and helped to improve the clarity of the manuscript.

References

Abelmann, A., Gersonde, R., 1991. Biosiliceous particle flux in the Southern Ocean. Mar. Chem. 35, 503–536. doi:10.1016/S0304-4203(09)90040-8

André, L., Cardinal, D., Alleman, L.Y., Moorbath, S., 2006. Silicon isotopes in ~3.8 Ga West Greenland rocks as clues to the Eoarchaean supracrustal Si cycle. Earth Planet. Sci. Lett. 245, 162–173. doi:10.1016/j.epsl.2006.02.046

Baah, C. a., Baah, J.I., 2002. Polypropylene degradation in NaOH environments. Mater. Des. 23, 341–343. doi:10.1016/S0261-3069(01)00091-7

Barker, P.F., Kennett, J.P., Al., E., 1988. Proc. ODP, Initial Reports 113. College Station. doi:doi:10.2973/odp.proc.ir.113.106.1988

Basile-Doelsch, I., Meunier, J.D., Parron, C., 2005. Another continental pool in the terrestrial silicon cycle. Nature 433, 399–402. doi:10.1038/nature03217

Bohrmann, G., Abelmann, A., Gersonde, R., Hubberten, H., Kuhn, G., 1994. Pure siliceous ooze, a diagenetic environment for early chert formation. Geology 22, 207–210.

Bohrmann, G., Kuhn, G., Abelmann, A., Gersonde, R., Fütterer, D., 1990. A young porcellanite occurrence from the Southwest Indian Ridge. Mar. Geol. 92, 155–163. doi:10.1016/0025-3227(90)90034-H

Bohrmann, G., Spiel, V., Hinze, H., Kuhn, G., 1992. Reflector " Pc " a prominent feature in the Maud Rise sediment sequence (eastern Weddell Sea): Occurrence, regional distribution and implications to silica diagenesis. Mar. Geol. 106, 69–87.

Botz, R., Bohrmann, G., 1991. Low-temperature opal-CT precipitation in Antarctic deep-sea sediments: evidence from oxygen isotopes. Earth Planet. Sci. Lett. 107, 612–617. doi:10.1016/0012-821X(91)90105-Q

Bramlette, M.N., 1946. Monterrey Formation of California and origin of its siliceous rocks. USGS Prof. Pap. 212, 57.

Brzezinski, M. a., Nelson, D.M., 1995. The annual silica cycle in the Sargasso Sea near Bermuda. Deep. Res. Part I Oceanogr. Res. Pap. 42, 1215–1237. doi:10.1016/0967-0637(95)93592-3

Cardinal, D., Alleman, L.Y., Dehairs, F., Savoye, N., Trull, T.W., André, L., 2005. Relevance of silicon isotopes to Si-nutrient utilization and Si-source assessment in Antarctic waters. Global Biogeochem. Cycles 19. doi:10.1029/2004GB002364

Chakrabarti, R., Fischer, W.W., Knoll, A.H., Jacobsen, S.B., 2012. Si isotope variability in Proterozoic cherts. Geochim. Cosmochim. Acta 91, 187–201. doi:10.1016/j.gca.2012.05.025

Cornelis, J.T., Weis, D., Lavkulich, L., Vermeire, M.L., Delvaux, B., Barling, J., 2014. Silicon isotopes record dissolution and re-precipitation of pedogenic clay minerals in a podzolic soil chronosequence. Geoderma 235-236, 19–29. doi:10.1016/j.geoderma.2014.06.023

De La Rocha, C.L., Brzezinski, M.A., DeNiro, M.J., 1997. Fractionation of silicon isotopes by marine diatoms during biogenic silica formation. Geochim. Cosmochim. Acta 61, 5051–5056.

De La Rocha, C.L., Brzezinski, M.A., DeNiro, M.J., 2000. A first look at the distribution of the stable isotopes of silicon in natural waters. Geochim. Cosmochim. Acta 64, 2467–2477.

Demarest, M.S., Brzezinski, M. a., Beucher, C.P., 2009. Fractionation of silicon isotopes during biogenic silica dissolution. Geochim. Cosmochim. Acta 73, 5572–5583. doi:10.1016/j.gca.2009.06.019

Dixit, S., Van Cappellen, P., van Bennekom, A.J., 2001. Processes controlling solubility of biogenic silica and pore water build-up of silicic acid in marine sediments. Mar. Chem. 73, 333–352. doi:10.1016/S0304-4203(00)00118-3

Egan, K.E., Rickaby, R.E.M., Leng, M.J., Hendry, Katharine, R., Hermoso, M., Sloane, H.J., Bostock, H., Halliday, A.N., 2012. Diatom Silicon Isotopes as a Proxy for Silicic Acid Utilisation : a Southern Ocean Core Top Calibration. Geochim. Cosmochim. Acta 96, 174–192. doi:10.1016/j.gca.2012.08.002

Ehlert, C., Grasse, P., Mollier-Vogel, E., Böschen, T., Franz, J., de Souza, G.F., Reynolds, B.C., Stramma, L., Frank, M., 2012. Factors controlling the silicon isotope distribution in waters and surface sediments of the Peruvian coastal upwelling. Geochim. Cosmochim. Acta 99, 128–145. doi:10.1016/j.gca.2012.09.038

Fan, H., Wen, H., Zhu, X., Hu, R., Tian, S., 2013. Hydrothermal activity during Ediacaran–Cambrian transition: Silicon isotopic evidence. Precambrian Res. 224, 23–35. doi:10.1016/j.precamres.2012.09.004

Gehlen, M., Beck, L., Calas, G., Flank, A.-M.-M., van Bennekom, A.J., Van Beusekom, J.E.E., Beck, L., Calas, G., Van Beusekom, J.E.E., Flank, A.-M.-M., van Bennekom, A.J., Van Beusekom, J.E.E., 2002. Unraveling the atomic structure of biogenic silica: Evidence of the structural association of Al and Si in diatom frustules. Geochim. Cosmochim. Acta 66, 1601–1609.

Geilert, S., Vroon, P.Z., Roerdink, D.L., Cappellen, P. Van, van Bergen, M.J., 2014. Silicon isotope fractionation during abiotic silica precipitation at low temperatures: inferences from flow-through experiments. Geochim. Cosmochim. Acta. doi:10.1016/j.gca.2014.07.003

Georg, R.B., Reynolds, B.C., Frank, M., Halliday, A.N., 2006. New sample preparation techniques for the determination of Si isotopic compositions using MC-ICPMS. Chem. Geol. 235, 95–104. doi:10.1016/j.chemgeo.2006.06.006

Hesse, R., 1988. Origin of chert: Diagenesis of biogenic siliceous sediments. J. Geol. Assoc. Canada 15, 171–192.

Hinman, N.W., 1990. Chemical factors influencing the rates and sequences of silica phase transitions : Effects of organic constituents. Geochim. Cosmochim. Acta 54, 1563–1574.

Hinman, N.W., 1998. Sequences of silica phase transitions: effects of Na, Mg, K, Al, and Fe ions. Mar. Geol. 147, 13–24. doi:10.1016/S0025-3227(98)00002-4

Hurd, D.C., 1973. Interactions of biogenic opal, sediment and seawater in the Central Equatorial Pacific. Geochim. Cosmochim. Acta 37, 2257–2282. doi:10.1016/0016-7037(73)90103-8

Isaacs, C.M., 1982. Influence of rock composition on kinetics of silica phase changes in the Monterey Formation, Santa Barbara area, California. Geology 10, 304.

Jochum, K.P., Nohl, U., Herwig, K., Lammel, E., Stoll, B., Hofmann, A.W., 2005. GeoReM: A New Geochemical Database for Reference Materials and Isotopic Standards. Geostand. Geoanalytical Res. 29, 333–338. doi:10.1111/j.1751-908X.2005.tb00904.x

Kastner, M., Keene, J.B., Gieskes, J.M., 1977. Diagenesis of siliceous oozes-I. Chemical controls on the rate of opal-A to opal-CT transformation- an experimental study. Geochim. Cosmochim. Acta 41, 1041–1059.

Kidder, D.L., Erwin, D.H., 2001. Secular Distribution of Biogenic Silica through the Phanerozoic : Comparison of Silica-Replaced Fossils and Bedded Cherts at the Series Level. J. Geol. 109, 509–522.

Marin-Carbonne, J., Chaussidon, M., Boiron, M.-C., Robert, F., 2011. A combined in situ oxygen, silicon isotopic and fluid inclusion study of a chert sample from Onverwacht Group (3.35Ga, South Africa): New constraints on fluid circulation. Chem. Geol. 286, 59–71. doi:10.1016/j.chemgeo.2011.02.025

Marin-Carbonne, J., Chaussidon, M., Robert, F., 2012. Micrometer-scale chemical and isotopic criteria (O and Si) on the origin and history of Precambrian cherts: Implications for paleo-temperature reconstructions. Geochim. Cosmochim. Acta 92, 129–147. doi:10.1016/j.gca.2012.05.040

Marin-Carbonne, J., Faure, F., Chaussidon, M., Jacob, D., Robert, F., 2013. A petrographic and isotopic criterion of the state of preservation of Precambrian cherts based on the characterization of the quartz veins. Precambrian Res. 231, 290–300. doi:10.1016/j.precamres.2013.03.019

Michalopoulos, P., Aller, R.C., 2004. Early diagenesis of biogenic silica in the Amazon delta: alteration, authigenic clay formation, and storage. Geochim. Cosmochim. Acta 68, 1061–1085. doi:10.1016/j.gca.2003.07.018

Michalopoulos, P., Aller, R.C., Reeder, R.J., 2000. Conversion of diatoms to clays during early diagenesis in tropical , continental shelf muds. Geology 28, 1095–1098. doi:10.1130/0091-7613(2000)28<1095:CODTCD>2.0.CO;2

Murata, K.J., Friedman, I., Gleason, J.D., 1977. Oxygen isotope relations between diagenetic silica minerals in Monterey Shale, Temblor Range, California. Am. J. Sci. 277, 259–272.

Murata, K.J., Nakata, J.K., 1974. Cristobalitic stage in the diagenesis of diatomaceous shale. Science 184, 567–568. doi:10.1126/science.184.4136.567

Oelze, M., von Blanckenburg, F., Bouchez, J., Hoellen, D., Dietzel, M., 2015. The effect of Al on Si isotope fractionation investigated by silica precipitation experiments. Chem. Geol. 397, 94–105. doi:10.1016/j.chemgeo.2015.01.002

Oelze, M., von Blanckenburg, F., Hoellen, D., Dietzel, M., Bouchez, J., 2014. Si stable isotope fractionation during adsorption and the competition between kinetic and equilibrium isotope fractionation: implications for weathering systems. Chem. Geol. 380, 161–171.

Ragueneau, O.G., Tréguer, P.J., Leynaert, A., Anderson, R.F., Brzezinski, M.A., DeMaster, D.J., Dugdale, R.C., Dymond, J., Fischer, G., Francois, R., Heinze, C., Maier-Reimer, E., Martin-Jézéquel, V., Nelson, D.M., Quéguiner, B., 2000. A review of the Si cycle in the modern ocean: recent progress and missing gaps in the application of biogenic opal as a paleoproductivity proxy. Glob. Planet. Change 26, 317–365.

Reynolds, B.C., Frank, M., Halliday, A., 2006. Silicon isotope fractionation during nutrient utilization in the North Pacific. Earth Planet. Sci. Lett. 244, 431–443. doi:10.1016/j.epsl.2006.02.002

Rickert, D., Schlüter, M., Wallmann, K., 2002. Dissolution kinetics of biogenic silica from the water column to the sediments. Geochim. Cosmochim. Acta 66, 439–455.

Roerdink, D.L., van den Boorn, S.H.J.M., Geilert, S., Vroon, P.Z., van Bergen, M.J., 2015. Experimental constraints on kinetic and equilibrium silicon isotope fractionation during the formation of non-biogenic chert deposits. Chem. Geol. 402, 40–51. doi:10.1016/j.chemgeo.2015.02.038

Schlich, R., Wise, S.W., Al., E., 1989. Proc. ODP, Initial Reports 120. College Station. doi:doi:10.2973/odp.proc.ir.120.1989

Schoenberg, R., von Blanckenburg, F., 2005. An assessment of the accuracy of stable Fe isotope ratio measurements on samples with organic and inorganic matrices by high-resolution multicollector ICP-MS. Int. J. Mass Spectrom. 242, 257–272. doi:10.1016/j.ijms.2004.11.025

Schuessler, J.A., von Blanckenburg, F., 2014. Testing the limits of micro-scale analyses of Si stable isotopes by femtosecond laser ablation multicollector inductively coupled plasma mass spectrometry with application to rock weathering. Spectrochim. Acta Part B At. Spectrosc. 98, 1–18. doi:10.1016/j.sab.2014.05.002

Steinhoefel, G., Horn, I., von Blanckenburg, F., 2009. Micro-scale tracing of Fe and Si isotope signatures in banded iron formation using femtosecond laser ablation. Geochim. Cosmochim. Acta 73, 5343–5360. doi:10.1016/j.gca.2009.05.037

Steinhoefel, G., von Blanckenburg, F., Horn, I., Konhauser, K.O., Beukes, N.J., Gutzmer, J., 2010. Deciphering formation processes of banded iron formations from the Transvaal and the Hamersley successions by combined Si and Fe isotope analysis using UV femtosecond laser ablation. Geochim. Cosmochim. Acta 74, 2677–2696. doi:10.1016/j.gca.2010.01.028

Sutton, J.N., Varela, D.E., Brzezinski, M. a., Beucher, C.P., Varela, D.E., Brzezinski, M.A., Beucher, C.P., 2013. Species-dependent silicon isotope fractionation by marine diatoms. Geochim. Cosmochim. Acta 104, 300–309. doi:10.1016/j.gca.2012.10.057

Tréguer, P.J., Nelson, D.M., Vanbennekom, a J., De Master, D.J., Leynaert, A., Quéguiner, B., 1995. The Silica Balance in the World Ocean: A Reestimate. Science 268, 375–379.

van Bennekom, A.J., Buma, A.G.J., Nolting, R.F., 1991. Dissolved aluminium in the Weddell-Scotia Confluence and effect of Al on the dissolution kinetics of biogenic silica. Mar. Chem. 35, 423–434. doi:10.1016/S0304-4203(09)90034-2

van Beusekom, J.E.E., van Bennekom, A.J., Tréguer, P.J., Morvan, J., 1997. Aluminium and silicic acid in water and sediments of the Enderby and Crozet Basins. Deep. Res. II 44, 987–1003.

Van Cappellen, P., Qiu, L., 1997a. Biogenic silica dissolution in sediments of the Southern Ocean. I. Solubility. Deep. Res. II 44, 1109–1128.

Van Cappellen, P., Qiu, L., 1997b. Biogenic silica dissolution in sediments of the Southern Ocean. II. Kinetics. Deep Sea Res. Part II Top. Stud. Oceanogr. 44, 1129–1149. doi:10.1016/S0967-0645(96)00112-9

van den Boorn, S.H.J.M., van Bergen, M.J., Nijman, W., Vroon, P.Z., 2007. Dual role of seawater and hydrothermal fluids in Early Archean chert formation: Evidence from silicon isotopes. Geology 35, 939. doi:10.1130/G24096A.1

van den Boorn, S.H.J.M., van Bergen, M.J., Vroon, P.Z., de Vries, S.T., Nijman, W., 2010. Silicon isotope and trace element constraints on the origin of ~3.5Ga cherts: Implications for Early Archaean marine environments. Geochim. Cosmochim. Acta 74, 1077–1103. doi:10.1016/j.gca.2009.09.009

Walther, J. V., Helgeson, H.C., 1977. Calculation of the thermodynamic properties of aqueous silica and the solubility of quartz and its polymorphs at high pressures and temperatures. Am. J. Sci. 277, 1315–1351.

Weaver, F.M., Wise, S.W., 1973. Early diagenesis of deep sea bedded chert. Antarct. J. Sep.-Oct., 298–300.

Wetzel, F., de Souza, G.F., Reynolds, B.C., 2014. What controls silicon isotope fractionation during dissolution of diatom opal? Geochim. Cosmochim. Acta 131, 128–137. doi:10.1016/j.gca.2014.01.028

Williams, L.A., Crerar, D.A., 1985. Silica Diagenesis, II. General Mechanisms. J. Sediment. Petrol. 55, 312–321.

Williams, L.A., Parks, G.A., Crerar, D.A., 1985. Silica Diagenesis, I. Solubility Controls. J. Sediment. Petrol. 55, 301–311.

Ziegler, K., Chadwick, O.A., Brzezinski, M.A., Kelly, E.F., 2005. Natural variations of δ30Si ratios during progressive basalt weathering, Hawaiian Islands. Geochim. Cosmochim. Acta 69, 4597–4610. doi:10.1016/j.gca.2005.05.008

Ziegler, K., Dodd, J.P., Sharp, Z.D., Brearley, A.J., Young, E.D., 2011. Silicon and oxygen isotope values of cherts and their precursors, in: Goldschmidt Conference Abstracts. p. 2284.

Ziegler, K., Marin-Carbonne, J., 2012. Silicon and oxygen isotopes during diagenesis of the Monterey chert, in: Goldschmidt Conference Abstracts. p. 2603.

Online Supplementary Material

The supplementary information includes detailed descriptions of analytical conditions (S1), Si isotope data of samples and reference materials (S2).

S1 Analytical methods

S1.1 Solution MC-ICP-MS silicon isotope analyses

Isotope ratios were determined in either medium or high resolution mode on a Thermo Neptune multi-collector inductively coupled plasma mass spectrometer (MC-ICP-MS) equipped with a Neptune Plus Jet Interface (using a Pfeiffer OnToolBooster interface pump; Jet sample and H skimmer cones). Samples and standards were diluted in 0.1 M HCl to between 0.35 and 0.7 ppm Si. In order to correct for mass bias drift, Mg (Alfa Aesar Specpure 14430) was added and adjusted to match Si concentrations. The solutions were aspirated by a PFA nebulizer with uptake rates of 80 to 120 µL/min and introduced into an ESI APEX desolvator. Silicon isotope signals ($^{28}Si^{+}$, $^{29}Si^{+}$, $^{30}Si^{+}$) were measured simultaneously on the interference-free low mass side of the peak for 30 cycles, alternating between Si isotopes and Mg isotopes in dynamic mode (with idle time of 3 s between magnet jumps) with an integration time of 4 s for each cycle. These conditions yielded sample signal intensities of 15 to 20 V for ^{28}Si at resolution of 3700 to 7700 (mass resolving power Δm/m) on a Faraday cup (10^{11} Ω) and 32-42 V for ^{24}Mg. Background intensities (typically 15 to 30 mV ^{28}Si) were measured on-peak in 0.1 M HCl containing Mg at a concentration matched to the samples and were subtracted from sample Si signal intensities. Temporal changes in instrumental mass bias on Si isotope ratios were corrected by $^{25}Mg/^{24}Mg$ drift correction employing the exponential mass bias law (Cardinal et al., 2003) and subsequent mass bias correction by sample-standard bracketing using concentration-matched NBS-28 as measurement standard. Measured isotope ratios were rejected when the mass bias drift, i.e. the change in the isotope ratio between two bracketing NBS-28 measurement, exceeded 0.2‰ in $^{30}Si/^{28}Si$ or $^{29}Si/^{28}Si$. In every measurement session, the Si isotope composition of several reference materials including BHVO-2, Diatomite, IRMM-017, and BigBatch was determined to evaluate precision and accuracy (Tab. S.6). We report isotope ratios as per mill deviation ($\delta \cdot 10^3$) from the international reference material NBS-28 in the delta notation:

$$\delta^{(x/28)}Si = \left[\frac{\left(\frac{xSi}{28Si}\right)_{sample}}{\left(\frac{xSi}{28Si}\right)_{NBS28}} - 1\right] \qquad \text{[Eq. S.1]}$$

where x denotes either ^{29}Si or ^{30}Si.

We report average δ-values obtained from 1 to 6 replicate measurements of the same analyte solution together with their 95% confidence interval (= t·SD/√n), which indicates the instrument repeatability (Table S.1). However, the uncertainty associated with the reported Si isotope results also contains uncertainty contributions from sample preparation, dissolution, column separation, and MC-ICP-MS analyses, which was evaluated as follows. In every measurement session, the Si isotope composition of several reference materials including BHVO-2, Diatomite, IRMM-017, and BigBatch was determined

(Table S.7). The δ-values and their 95%CI are 0.64 ± 0.01‰ δ^{29}Si, 1.24 ± 0.02‰ δ^{30}Si for Diatomite (n= 13); -0.68 ± 0.02‰ δ^{29}Si, -1.34 ± 0.03‰ δ^{30}Si for IRMM-017 (n= 14); -5.45 ± 0.01‰ δ^{29}Si, -10.69 ± 0.03‰ δ^{30}Si for Big Batch (n= 18); -0.06 ± 0.02‰ δ^{29}Si, -0.14 ± 0.03‰ δ^{30}Si for 'Herasil' SiO_2 glass (an in-house standard); n= 15); -0.15 ± 0.03‰ δ^{29}Si, -0.30 ± 0.05‰ δ^{30}Si for BHVO-2 (n= 7). Based on evaluation of accuracy and precision of the sample repeat measurements and comparison of results obtained on reference materials during this study with published data compiled in Jochum et al. (2005; Table S.6), the uncertainty of the entire solution MC-ICP-MS method is estimated to be ± 0.07‰ (2SD) for δ^{29}Si and ± 0.10‰ (2SD) for δ^{30}Si. The same estimate was obtained by statistical evaluation according to equation 2 in Schoenberg and von Blanckenburg (2005), based on repeat analyses of all samples analyzed in this study. This uncertainty is used for data interpretation in this study.

S1.2 Femtosecond-LA-MC-ICP-MS analyses of silicon isotopes and Al/Si ratios

The micro-scale silicon isotope composition was determined on three samples (PS-2089-2-600P, PS2070-1-472P and PS2070-1-472-bh) of porcellanite (opal-CT) by UV femtosecond laser ablation MC-ICP-MS (UV fsLA-MC-ICP-MS, *Fem2*) at GFZ Potsdam. Analytical conditions are briefly described below and further details on the instrumentation and analytical method are described in Schuessler and von Blanckenburg (2014).

Porcellanite samples were embedded in epoxy resin and polished thin sections of 30 µm thickness were prepared for laser ablation analyses. Reference materials for calibration and for analytical quality control (NIST 8546 aka NBS-28 quartz, USGS BHVO-2G basalt glass, IRMM-017 Si single crystal) were prepared as polished epoxy grain mounts and placed together with samples into the ablation cell. Helium was used as carrier gas for the ablated material, which was mixed with Ar/H_2O from spraychamber nebulization of Milli-Q-H_2O before entering the ICP source of the mass spectrometer.

The UV laser beam (196 nm, <200 fs pulses) was focused beneath the sample surface to obtain a spot diameter between 18 and 25 µm at a fluence of 3 to 1.5 J/cm². At each location ablation was done in raster scanning mode (40 µm/s scan speed), ablating a surface area of about 100 x 100 µm with less than 10 µm crater depth, representing a volume of less than 10^{-4} mm^3. Due to the more irregular shape of NBS-28 quartz crystals, line scans were used to ablate an equivalent volume for analyses. Laser pulse repetition rates between 5 and 50 Hz were employed, depending the Si concentrations and ablation properties of the different materials to obtain Si signal intensities of 5 to 8 V on ^{28}Si (10^{11} Ω amplifiers), matched within 20% relative to signals from NBS-28 ablation, which was used for standard-sample-standard bracketing. The Faraday multi collector setting of the Neptune mass spectrometer was aligned to simultaneously detect $^{28}Si^+$, $^{29}Si^+$, $^{30}Si^+$, and $^{27}Al^+$, and to resolve interferences produced by molecular oxides.

Each individual Si isotope ratio measurement consists of the mean of 80 1-second integration cycles corrected by on-peak subtraction of the background measured at the beginning of a sequence (< 43 mV ^{28}Si). Data evaluation followed the protocol described in Schuessler and von Blanckenburg (2014). All time-resolved data were screened to detect potentially occurring irregular mass bias drift, and interferences (in a three-isotope-plot). Outliers beyond the 3σ limits of a Gaussian normal distribution

were excluded, typically affecting no more than five of 80 cycles. We report results in the δ notation as per mil deviation relative to NBS-28 together with the internal standard error of the mean (2SE) of single sample measurements (Tables: S.2, S.3, S.4), which is typically <0.1‰ for $\delta^{30}Si$ as calculated by error propagation from measurements of one sample and two bracketing NBS-28 standards. In the analytical session in which sample PS2089-2-600P was analyzed, we experienced a higher signal of $^{16}O^{14}N^+$ (close to the mass of $^{30}Si^+$) as compared to the other analytical sessions. In medium mass resolution mode of the Neptune, $^{30}Si^+$ can be accurately measured on the interference-free peak shoulder, where $^{30}Si^+$ is resolved from $^{16}O^{14}N^+$ (Schuessler and von Blanckenburg, 2014). However, if the signal intensity of $^{16}O^{14}N^+$ becomes unfavorably high relative to the $^{30}Si^+$ signal, tailing of the $^{16}O^{14}N^+$ peak towards $^{30}Si^+$ leads to a much narrower $^{30}Si^+$ plateau and small magnet instabilities then result in inaccuracies in the $^{30}Si/^{28}Si$ ratio and also higher uncertainties in this ratio associated with the on-peak blank correction (Schuessler and von Blanckenburg, 2014). Therefore, we chose not to use the $\delta^{30}Si$ values from this analytical session for sample PS2089-2-600P, but instead evaluated the $\delta^{29}Si$ values. $\delta^{29}Si$ was not affected by tailing from increased molecular interference signals because the $^{14}N^{14}N^1H^+/^{29}Si^+$ signal ratio was < 0.3, $^{14}N^{14}N^+/^{28}Si^+$ signal ratio was < 0.02, compared to a $^{14}N^{16}O^+/^{30}Si^+$ signal ratio of > 30. For this session we have converted measured $\delta^{29}Si$ values into $\delta^{30}Si$ following the mass-dependent isotope fractionation law $\delta^{30}Si$ (calculated) = 1.96 · $\delta^{29}Si$ (Table S.2). For these measurements we estimated the internal uncertainty in individual $\delta^{30}Si$ (calculated) values by multiplication of the internal standard error of the mean (2SE) of measured $\delta^{29}Si$ by 1.5 (see Table S.2). As the count-statistical uncertainties in $\delta^{29}Si$ and $\delta^{30}Si$ ratios are correlated (Schuessler and von Blanckenburg, 2014), we obtained this factor of 1.5 from the two other independent analytical sessions reported in Tables S.3 and S.4. This approach is supported by comparing the measured $\delta^{30}Si$ values with $\delta^{30}Si$ (calc) values in Tables S.2 which gave differences typically less than 0.1‰, which is within uncertainty of the fsLA-MC-ICP-MS method. The uncertainty of the fsLA-MC-ICP-MS method (external long-term repeatability) is ± 0.15‰ (2SD) for $\delta^{29}Si$ and ± 0.23‰ (2SD) for $\delta^{30}Si$, respectively (Schuessler and von Blanckenburg, 2014), and these uncertainties should be applied for geological interpretation and comparison to results obtained in other laboratories. Accuracy was verified by measurements of reference materials during each analytical session (Tab. S.7). During this study we obtained a mean $\delta^{30}Si$ of -0.24 ± 0.34‰ (2SD, n= 26) for BHVO-2 and -1.28 ± 0.26‰ (2SD, n= 17) for IRMM-017, respectively, which agrees well within uncertainties to previously published values (e.g. Reynolds et al., 2007; Savage et al., 2014; Chmeleff et al., 2008; Schuessler and von Blanckenburg, 2014).

To determine Al concentrations along the LA transects in the porcellanite and opal-CT samples, $^{27}Al/^{28}Si$ ratios were measured simultaneously with Si isotope ratios at a precision of about 2% (2SD). To obtain Al/Si mass ratios, calibration was done by measurements on BHVO-2G, having an Al/Si mass ratio of 0.3123 ± 0.0061 (GeoReM compiled value; Jochum et al., 2005) and Si was used as internal reference element to determine Al concentrations. The fsLA-MC-ICP-MS repeatability of Al/Si weight ratios on the reference material BHVO-2G is 0.3131 ± 0.0081 (2SD, n= 30). However, the major uncertainty contribution for Al quantification in the porcellanites stems from spatial variability in Si

contents (used as internal standard), which was estimated for different samples to be 1% (PS2089-2-600P), 7% (PS2070-1-472P), and 15% (PS2070-1-472-bh), derived by comparison of LA Si signal intensities at different parts of the porcellanite layers. Thus, the *in-situ* Al concentration can be determined with a relative precision of up to 6% (PS2089-2-600P), 9% (PS2070-1-472P), and 16% (PS2070-1-472-bh) at 95% confidence level, using the Si concentration of the bulk porcellanite (determined by ICP-OES after dissolution) as internal reference.

S1.3 Concentration measurements by ICP-OES

Element concentrations were determined on diluted sample aliquots after solid sample digestions (as described in the main text section 2.2.2) using an axial ICP-OES (Varian 720-ES). The instrument was calibrated using 5 multi-element ICP standard solutions in 0.3 M HNO_3 matrix, ranging from 0.01 ppm to 10 ppm Si and from 0.002 to 1 ppm of other elements. The matrix of the calibration standards was matched to Na concentrations in sample solutions. The instrumental precision of ICP-OES analyses on diluted solutions is typically better than 5% relative. However, in this study the overall uncertainty in reported concentration data for solid samples can be higher due to the sample preparation method designed specifically for Si isotope ratio measurements, where precise knowledge of sample weight is not necessary. For example, sample amounts of <15 mg, that have not been dried to remove adsorbed ambient water lead to imprecise weighing and hence inferior relative uncertainties of up to 15% for reported element concentrations. This level of uncertainty was estimated from measurements of reference materials (e.g., BHVO-2G, NBS28) following the same dissolution procedure as for the samples.

S2 Silicon isotope data

Supplementary Tables S.1 – S.9

Table S.1: Solution MC-ICP-MS silicon isotope data of bulk Pleistocene (PS2089-2) and Pliocene (PS2070-1) siliceous sediments and porcellanites. Each sample is representative of ca. 1 cm sediment. Average δ-values of n replicate measurements and their 95% confidence intervals (= t·SD/√n) are reported. 95%CI indicates the intermediate precision of the mass spectrometric method (instrument repeatability). The overall uncertainty of the solution MC-ICP-MS method is estimated to be ± 0.07‰ (2SD) for $\delta^{29}Si$ and ± 0.10‰ (2SD) for $\delta^{30}Si$.

sample	depth below seafloor [cm]	$\delta^{29}Si$ [‰]	95%CI	$\delta^{30}Si$ [‰]	95%CI	n
PS2089-2 541	541	0.67	0.04	1.27	0.04	4
PS2089-2 549	549	0.62	0.07	1.23	0.06	5
PS2089-2 559	559	0.57	0.07	1.06	0.07	4
PS2089-2 589	589	0.70	0.06	1.31	0.06	4
PS2089-2 596	596	0.34	0.05	0.64	0.06	5
PS2089-2 600P porous	600	0.88	0.02	1.69	0.07	4
PS2089-2 600P dense	600	0.99	0.07	1.96	0.07	3
PS2089-2 617	617	0.76	0.02	1.50	0.06	5
PS2089-2 628	628	0.65	0.06	1.28	0.08	4
PS2089-2 639	639	0.55	0.04	1.09	0.05	4
PS2089-2 670	670	0.11	0.05	0.22	0.18	3
PS2089-2 700	700	0.21	0.06	0.42	0.10	5
PS2089-2 730	730	0.07	0.03	0.16	0.06	4
PS2070-1-423	423	0.26	0.05	0.51	0.07	5
PS2070-1-428	428	0.18	0.04	0.35	0.12	4
PS2070-1-432	432	0.12	0.05	0.24	0.11	6
PS2070-1-438	438	0.16	0.05	0.32	0.08	4
PS2070-1-443	443	0.10	0.01	0.18	0.07	4
PS2070-1-448	448	0.01	0.04	0.03	0.04	4
PS2070-1-453	453	-0.09	0.02	-0.12	0.05	4
PS2070-1-457	457	-0.15	0.05	-0.28	0.04	4
PS2070-1-463	463	-0.08	0.04	-0.15	0.08	3
PS2070-1-467	467	-0.11	0.09	-0.18	0.12	5
PS2070-1-471	471	-0.17	0.03	-0.34	0.05	5
PS2070-1-472P	472	1.17	0.06	2.28	0.14	4
PS2070-1-475	475	-0.08	0.05	-0.15	0.06	4
PS2070-1-479	479	0.11	0.05	0.20	0.05	5
PS2070-1-483	483	0.03	0.03	0.04	0.06	5
PS2070-1-487	487	-0.15	0.03	-0.28	0.06	6
PS2070-1-493	493	-0.08	0.06	-0.15	0.08	5
PS2070-1-498	498	0.05	0.05	0.07	0.10	5
PS2070-1-503	503	-0.03	0.07	-0.01	0.07	3
PS2070-1-508	508	-0.08	0.05	-0.13	0.05	3
PS2070-1-513	513	-0.03	0.02	-0.08	0.06	4
PS2070-1-517	517	-0.12	0.10	-0.26	0.13	3
PS2070-1-527	527	-0.04	0.05	-0.09	0.07	4
PS2070-1-564	564	0.29	0.07	0.61	0.08	5
PS2070-1-613	613	0.22	0.08	0.47	0.09	5

Table S.2: fs-LA-MC-ICP-MS silicon isotope and Al/Si data of porcellanite layer PS2089-2-600P. $\delta^{30}Si$ values were calculated from $\delta^{29}Si$ (assuming $\delta^{30}Si = 1.96 \cdot \delta^{29}Si$, see text above). The internal standard error of the mean (2SE) is given for each individual sample measurement (n= 80 integrations á 1 second). The uncertainty of the fsLA-MC-ICP-MS method (external long-term repeatability) is ± 0.15‰ (2SD) for $\delta^{29}Si$ and ± 0.23 ‰ (2SD) for $\delta^{30}Si$, respectively.

analysis ID	dist. [mm]	$\delta^{29}Si$ [‰]	2SE	$\delta^{30}Si$ calc. [‰]	2SE calc	$\delta^{30}Si$ [‰]	$^{27}Al/^{28}Si$ $*10^{-3}$	2SE [a] $*10^{-3}$	Al [ppm]	± [b]	Al/Si $*10^{-3}$ [wt%/wt%]
600P_1.1	0.10	0.85	0.08	1.67	0.12	1.52	6.6	0.56	1227	120	2.9
600P_2	0.35	0.76	0.08	1.49	0.13	1.66	7.9	0.42	1473	104	3.5
600P_3	0.55	0.71	0.09	1.39	0.13	1.62	9.1	0.81	1707	171	4.1
600P_4	0.75	0.83	0.08	1.62	0.11	1.60	7.7	0.81	1441	166	3.4
600P_5	0.95	0.84	0.08	1.66	0.12	1.72	7.2	0.51	1346	115	3.2
600P_6	1.20	0.79	0.08	1.56	0.12	1.62	15.5	1.68	2897	342	6.9
600P_7	1.40	0.77	0.09	1.51	0.14	1.44	8.4	0.69	1565	148	3.7
600P_7.1	1.40	0.64	0.09	1.26	0.14	1.30	7.0	1.19	1310	230	3.1
600P_8	1.60	0.79	0.10	1.55	0.14	1.46	12.9	1.10	2405	235	5.7
600P_9	1.85	0.79	0.16	1.56	0.24	1.46	7.8	0.73	1450	153	3.4
600P_11	2.25	0.73	0.09	1.44	0.13	1.62	6.0	0.51	1121	110	2.7
600P_12	2.45	0.78	0.08	1.53	0.11	1.61	5.5	0.38	1018	86	2.4
600P_13	2.65	0.87	0.08	1.71	0.12	1.81	6.5	0.57	1205	121	2.9
600P_14	2.90	0.95	0.08	1.87	0.12	2.04	5.0	0.31	939	74	2.2
600P_14.1	2.90	0.71	0.08	1.39	0.12	1.40	6.1	0.63	1145	130	2.7
600P_15	3.10	0.82	0.08	1.61	0.12	1.61	6.0	0.55	1114	115	2.6
600P_16	3.35	0.78	0.09	1.53	0.13	1.66	4.6	1.00	850	190	2.0
600P_17	3.60	0.74	0.09	1.46	0.13	1.57	8.6	0.80	1609	168	3.8
600P_18	3.80	0.88	0.08	1.73	0.12	1.74	5.7	0.70	1070	139	2.5
600P_19	4.00	0.82	0.08	1.62	0.12	1.73	6.5	0.66	1206	136	2.9
600P_20	4.25	0.76	0.08	1.50	0.12	1.58	7.4	0.64	1374	136	3.3
600P_20.1	4.25	0.62	0.09	1.21	0.14	1.42	7.2	1.17	1343	227	3.2
600P_21	4.45	0.79	0.08	1.55	0.13	1.40	14.0	1.68	2619	337	6.2
600P_22	4.65	0.69	0.08	1.35	0.12	1.39	9.6	0.78	1798	168	4.3
600P_23	4.85	0.91	0.09	1.79	0.14	1.60	9.3	1.13	1728	226	4.1
600P_24	5.15	0.73	0.09	1.44	0.13	1.68	9.6	0.99	1797	203	4.3
600P_25	5.35	0.74	0.12	1.45	0.18	1.76	10.3	1.03	1923	212	4.6
600P_26	5.50	0.79	0.13	1.56	0.19	1.82	9.5	0.68	1779	152	4.2
600P_27	5.70	0.68	0.14	1.33	0.21	1.57	9.1	1.09	1703	219	4.0
600P_28	5.95	0.68	0.10	1.34	0.15	1.53	8.6	1.12	1602	222	3.8
600P_29	6.15	0.75	0.08	1.46	0.12	1.63	7.6	0.82	1413	166	3.4
600P_30	6.40	0.78	0.09	1.54	0.14	1.73	7.9	0.91	1474	183	3.5
600P_31	6.65	0.66	0.09	1.29	0.13	1.59	9.5	0.77	1771	166	4.2
600P_32	6.80	0.67	0.09	1.32	0.13	1.58	8.1	0.73	1512	153	3.6
600P_32.1	6.80	0.66	0.08	1.30	0.12	1.37	7.1	1.01	1320	199	3.1
600P_33	6.95	0.84	0.08	1.64	0.13	1.58	6.4	0.38	1192	91	2.8
600P_34	7.25	0.92	0.08	1.81	0.12	1.79	6.1	0.47	1134	103	2.7
600P_34.1	7.25	0.65	0.09	1.27	0.13	1.37	9.0	1.02	1683	206	4.0
600P_35	7.45	1.03	0.09	2.02	0.14	2.10	4.5	0.29	840	66	2.0
600P_36	7.65	0.90	0.08	1.76	0.13	1.91	4.8	0.32	892	73	2.1
600P_37	7.95	0.96	0.08	1.88	0.13	2.00	4.5	0.21	832	56	2.0

Table S.2 cont.

analysis ID	dist. [mm]	$\delta^{29}Si$ [‰]	2SE	$\delta^{30}Si$ calc. [‰]	2SE calc	$\delta^{30}Si$ [‰]	$^{27}Al/^{28}Si$ $*10^{-3}$	2SE [a] $*10^{-3}$	Al [ppm]	± [b]	Al/Si $*10^{-3}$ [wt%/wt%]
600P_38	8.15	0.89	0.07	1.74	0.11	1.80	5.0	0.40	928	87	2.2
600P_39	8.35	0.90	0.08	1.77	0.12	1.79	5.0	0.28	935	68	2.2
600P_40	8.60	0.91	0.08	1.79	0.12	1.78	4.5	0.21	838	55	2.0
600P_41	8.80	1.02	0.09	2.01	0.14	1.92	4.5	0.34	836	75	2.0
600P_42.1	9.00	0.94	0.07	1.84	0.11	1.88	4.3	0.21	809	55	1.9
600P_44	9.45	0.98	0.10	1.94	0.15	1.98	6.1	0.50	1138	107	2.7
600P_45	9.60	0.93	0.10	1.82	0.15	1.77	5.0	0.54	933	110	2.2
600P_46	9.85	0.91	0.10	1.79	0.15	1.76	4.5	0.41	832	86	2.0
600P_47	10.05	0.92	0.10	1.81	0.15	1.82	4.1	0.41	759	84	1.8
600P_48	10.25	0.97	0.09	1.90	0.13	1.92	4.7	0.37	885	80	2.1
600P_49	10.45	0.92	0.08	1.80	0.12	1.91	4.3	0.50	799	101	1.9
600P_50	10.70	0.95	0.08	1.87	0.13	1.85	3.6	0.39	675	79	1.6
600P_50.1	10.70	0.95	0.07	1.86	0.11	1.89	3.4	0.20	636	48	1.5
600P_51	10.95	0.98	0.08	1.93	0.13	1.86	3.4	0.34	629	70	1.5
600P_52	11.15	0.88	0.08	1.73	0.12	1.74	4.7	0.48	878	99	2.1
600P_53	11.35	0.92	0.08	1.80	0.11	1.75	3.9	0.37	732	78	1.7
600P_54	11.55	0.98	0.07	1.93	0.11	1.96	2.4	0.39	452	77	1.1
600P_55	11.75	1.04	0.08	2.05	0.12	2.05	3.5	0.35	650	71	1.5
600P_56	12.00	1.05	0.09	2.07	0.13	2.17	6.1	0.31	1147	79	2.7
600P_56.1	12.00	1.02	0.08	2.01	0.11	2.09	5.0	0.29	937	69	2.2
600P_57	12.20	1.03	0.07	2.02	0.11	2.11	2.4	0.19	447	42	1.1
600P_58	12.40	0.96	0.07	1.88	0.10	2.05	3.3	0.20	614	48	1.5
600P_59	12.65	0.97	0.08	1.91	0.11	1.92	3.4	0.20	641	48	1.5
600P_60	12.85	0.94	0.07	1.84	0.11	1.87	3.8	0.29	704	63	1.7
600P_61	13.05	0.93	0.08	1.82	0.12	1.81	3.2	0.18	605	45	1.4
600P_62	13.25	0.91	0.08	1.78	0.12	1.67	2.5	0.44	466	84	1.1
600P_62.1	13.25	0.87	0.07	1.71	0.11	1.81	3.5	0.18	646	46	1.5
600P_63	13.45	0.80	0.09	1.58	0.13	1.65	4.9	0.47	913	98	2.2
600P_64	13.65	0.84	0.08	1.66	0.12	1.56	4.7	0.40	871	86	2.1
600P_65	13.85	0.73	0.09	1.44	0.14	1.56	20.6	0.80	3843	235	9.1
600P_65.1	13.85	0.81	0.07	1.60	0.11	1.69	18.3	0.79	3415	218	8.1

[a] uncertainty estimated from error propagation of internal counting statistical error and repeatability on BHVO-2G

[b] uncertainty estimated from error propagation of internal counting statistical error, repeatability on BHVO-2G, measurement uncertainty on Al/Si (BHVO-2G GeoRem reference value), uncertainty on the silicon concentration in the sample, and the variability in the silicon concentration of the sample

Table S.3: fs-LA-MC-ICP-MS silicon isotope and Al/Si data of porcellanite layer PS2070-1-472P. The internal standard error of the mean (2SE) is given for each individual sample measurement (comprising n= 80 integrations á 1 second for sample and 2 bracketing standards). The uncertainty of the fsLA-MC-ICP-MS method (external long-term repeatability) is ± 0.15‰ (2SD) for $\delta^{29}Si$ and ± 0.23‰ (2SD) for $\delta^{30}Si$, respectively.

analysis ID	distance [mm]	$\delta^{29}Si$ [‰]	2SE	$\delta^{30}Si$ [‰]	2SE	$^{27}Al/^{28}Si$ $*10^{-3}$	2SE [a] $*10^{-3}$	Al [ppm]	± [b]	Al/Si $*10^{-3}$ [wt%/wt%]
472P_1	0.1	1.26	0.09	2.49	0.12	1.4	0.12	<350		0.8
472P_2	0.2	1.29	0.08	2.58	0.10	0.4	0.03	<350		0.2
472P_3	0.3	1.32	0.07	2.51	0.10	0.1	0.02	<350		0.1
472P_4	0.4	1.23	0.08	2.39	0.10	0.0	0.01	<350		0.0
472P_5	0.5	1.29	0.07	2.65	0.09	0.1	0.01	<350		0.1
472P_6	0.6	1.39	0.08	2.82	0.10	0.1	0.03	<350		0.0
472P_7	0.7	1.45	0.07	2.77	0.11	0.4	0.04	<350		0.2
472P_8	0.8	1.48	0.07	2.89	0.09	0.3	0.05	<350		0.2
472P_9	0.9	1.38	0.07	2.76	0.10	0.3	0.03	<350		0.2
472P_10	1.0	1.50	0.07	2.95	0.10	0.4	0.02	<350		0.2
472P_11	1.1	1.38	0.07	2.82	0.10	0.4	0.04	<350		0.2
472P_12	1.2	1.43	0.07	2.80	0.11	0.3	0.02	<350		0.1
472P_13	1.3	1.47	0.07	2.92	0.10	0.6	0.07	<350		0.3
472P_14	1.4	1.37	0.07	2.65	0.10	0.2	0.02	<350		0.1
472P_15	1.5	1.40	0.08	2.87	0.11	0.8	0.05	<350		0.4
472P_16	1.6	1.23	0.07	2.47	0.10	8.2	0.40	1897	189	4.5
472P_17	1.7	1.09	0.07	2.12	0.10	10.5	0.52	2438	243	5.8
472P_18	1.8	1.12	0.07	2.18	0.10	10.2	0.72	2365	264	5.6
472P_19	1.9	1.22	0.07	2.35	0.11	15.5	0.78	3603	361	8.6
472P_20	2.0	1.23	0.07	2.35	0.09	6.1	0.24	1405	134	3.3
472P_21	2.1	1.23	0.08	2.36	0.11	5.7	0.22	1333	126	3.2
472P_22	2.2	1.28	0.07	2.41	0.10	5.3	0.51	1236	160	2.9
472P_23	2.3	1.28	0.07	2.40	0.12	3.8	0.18	878	87	2.1
472P_24	2.4	1.17	0.09	2.27	0.12	5.3	0.28	1227	124	2.9
472P_25	2.5	1.20	0.08	2.33	0.12	5.4	0.19	1247	117	3.0
472P_26	2.6	1.22	0.08	2.33	0.13	4.0	0.36	939	116	2.2
472P_27	2.7	1.24	0.07	2.40	0.14	12.2	0.63	2837	286	6.7
472P_28	2.8	1.24	0.07	2.37	0.12	14.8	0.48	3442	319	8.2
472P_29	2.9	1.27	0.08	2.45	0.13	25.6	0.87	5931	552	14.1
472P_30	3.0	1.31	0.11	2.56	0.17	11.0	0.37	2563	238	6.1
472P_31	3.1	1.25	0.12	2.50	0.20	12.0	0.70	2787	291	6.6
472P_32	3.2	1.22	0.12	2.43	0.20	6.9	0.32	1603	157	3.8
472P_33	3.3	1.14	0.09	2.19	0.15	4.0	0.20	919	92	2.2

[a] uncertainty estimated from error propagation of internal counting statistical error and repeatability on BHVO-2G

[b] uncertainty estimated from error propagation of internal counting statistical error, repeatability on BHVO-2G, measurement uncertainty on Al/Si (BHVO-2G GeoRem reference value), uncertainty on the silicon concentration in the sample, and the variability in the silicon concentration of the sample

Table S.4: fs-LA-MC-ICP-MS silicon isotope and Al/Si data of a porcellanite-filled animal burrow (ichnofossil; PS-2070-1-472-bh) in the vicinity of the porcellanite in piston core PS2070-1. The internal standard error of the mean (2SE) is given for each individual sample measurement (comprising n= 80 integrations á 1 second for sample and 2 bracketing standards). The uncertainty of the fsLA-MC-ICP-MS method (external long-term repeatability) is ± 0.15‰ (2SD) for δ^{29}Si and ± 0.23‰ (2SD) for δ^{30}Si, respectively.

analysis ID	distance [mm]	δ^{29}Si [‰]	2SE	δ^{30}Si [‰]	2SE	^{27}Al/^{28}Si *10^{-3}	2SE [a] *10^{-3}	Al [ppm]	± [b]	Al/Si *10^{-3} [wt%/wt%]
472P_bh6	0.5	1.18	0.15	2.21	0.25	8.4	0.40	671	112	1.53
472P_bh7	0.7	1.14	0.12	2.18	0.20	11.6	0.58	910	153	2.08
472P_bh8	0.8	1.14	0.11	2.20	0.17	6.9	0.27	557	92	1.27
472P_bh9	0.9	1.09	0.10	2.23	0.13	4.2	0.14	359	59	0.82
472P_bh10	1.1	1.17	0.10	2.41	0.15	6.5	0.16	533	87	1.22
472P_bh11	1.2	1.15	0.11	2.06	0.15	5.7	0.20	466	77	1.06
472P_bh12	1.3	1.10	0.10	2.21	0.15	6.6	0.21	535	87	1.22
472P_bh13	1.4	1.16	0.09	2.25	0.15	3.3	0.12	289	48	0.66
472P_bh14	1.6	1.09	0.09	2.21	0.13	1.2	0.09	<130		0.30
472P_bh15	1.8	1.13	0.10	2.21	0.14	1.2	0.08	<130		0.29
472P_bh16	1.9	1.11	0.09	2.23	0.13	1.2	0.08	<130		0.29
472P_bh17	2.1	1.21	0.09	2.41	0.14	2.7	0.13	242	41	0.55
472P_bh18	2.2	1.18	0.09	2.28	0.12	1.4	0.08	145	25	0.33
472P_bh19	2.4	1.15	0.10	2.32	0.14	1.4	0.06	146	24	0.33
472P_bh20	2.5	1.23	0.08	2.26	0.12	0.7	0.06	<130		0.20
472P_bh21	2.7	1.15	0.09	2.14	0.13	0.6	0.04	<130		0.19
472P_bh22	2.8	1.13	0.10	2.30	0.13	0.7	0.06	<130		0.20
472P_bh23	3.0	1.23	0.08	2.28	0.11	0.7	0.06	<130		0.20
472P_bh24	3.2	1.19	0.08	2.33	0.11	0.8	0.09	<130		0.21
472P_bh25	3.3	1.20	0.08	2.37	0.11	0.1	0.04	<130		0.10
472P_bh26	3.5	1.16	0.08	2.30	0.13	0.1	0.01	<130		0.08
472P_bh27	3.6	1.32	0.08	2.41	0.13	0.2	0.02	<130		0.11
472P_bh28	3.8	1.27	0.09	2.41	0.13	1.0	0.06	<130		0.25
472P_bh29	4.0	1.31	0.12	2.46	0.22	1.8	0.33	<130		0.43
472P_bh30	4.2	1.40	0.09	2.63	0.15	3.8	0.38	324	61	0.74
472P_bh31	4.3	1.36	0.11	2.60	0.12	1.8	0.22	166	34	0.38
472P_bh32	4.6	1.13	0.09	2.13	0.11	2.7	0.47	232	56	0.53
472P_bh33	5.0	1.17	0.09	2.22	0.12	0.9	0.07	<130		0.23
472P_bh34	5.3	1.20	0.09	2.43	0.15	0.7	0.06	<130		0.21
472P_bh35	5.4	1.23	0.09	2.45	0.13	1.1	0.06	<130		0.28
472P_bh36	5.6	1.27	0.09	2.35	0.16	1.2	0.04	<130		0.30
472P_bh39	6.2	1.19	0.09	2.44	0.14	3.6	0.15	304	50	0.69
472P_bh48	7.8	-0.03	0.14	-0.11	0.22	20.5	0.80	1580	261	3.61
472P_bh50	8.2	-0.07	0.16	-0.27	0.26	28.4	1.17	2181	362	4.98

[a] uncertainty estimated from error propagation of internal counting statistical error and repeatability on BHVO-2G

[b] uncertainty estimated from error propagation of internal counting statistical error, repeatability on BHVO-2G, measurement uncertainty on Al/Si (BHVO-2G GeoRem reference value), uncertainty on the silicon concentration in the sample, and the variability in the silicon concentration of the sample

Table S.5: Major- and trace element concentrations in bulk samples analyzed by ICP-OES (Varian 720-ES). Na concentrations were not measured because NaOH was used for sample digestion. The difference to 100% of the sum of the major oxides thus comprises Na, K, volatile compounds, organic matter as well as adhesively and structurally bound water in opal. The relative analytical uncertainty is estimated based on measurements of reference materials following the same dissolution protocol and is up to 15% relative.

	wt%						ppm			
sample name	**sediment depth [cm]**	**SiO_2**	**Al_2O_3**	**Fe_2O_3**	**MgO**	**CaO**	**Mn**	**La**	**Ba**	**Sr**
2089-2 541	541	74.4	1.1	1.1	0.7	2.6	<127	176	543	104
2089-2 549	549	73.0	1.9	1.4	0.8	1.7	<127	189	536	83
2089-2 559	559	67.6	3.5	3.3	1.0	1.8	<127	237	562	99
2089-2 589	589	75.6	0.3	0.2	0.5	0.2	<127	<115	269	27
2089-2 596	596	73.6	2.2	1.4	0.8	0.3	587	1089	4028	133
2089-2 600P1	600	87.3	1.9	1.3	0.4	0.6	<127	<115	193	27
2089-2 600P2	600	86.6	<0.3	<0.19	0.2	<0.09	<127	<115	<133	10
2089-2 617	617	72.4	0.3	0.8	0.8	0.3	<127	<115	268	37
2089-2 628	628	70.7	1.2	1.0	0.9	0.3	<127	134	327	47
2089-2 639	639	73.6	1.8	1.2	0.8	0.4	<127	156	469	48
2089-2 670	670	58.2	24.5	14.2	3.0	4.4	825	353	1031	170
2089-2 700	700	52.5	16.0	10.1	1.9	13.3	680	423	1191	378
2089-2 730	730	52.3	23.7	14.4	2.8	11.1	997	328	812	299
2070-1 423	423	73.9	3.0	2.1	0.8	0.3	594	1757	6439	189
2070-1 428	428	70.8	3.1	2.1	0.8	0.3	562	1791	6558	194
2070-1 432	432	72.4	2.9	2.1	0.8	0.3	599	1717	6287	189
2070-1 438	438	71.4	2.6	1.8	0.7	0.3	414	1588	5702	174
2070-1 443	443	73.0	1.8	1.3	0.6	0.2	296	1218	4350	141
2070-1 448	448	73.4	1.2	0.7	0.5	0.2	148	1078	3640	125
2070-1 453	453	71.9	1.0	0.6	0.6	0.2	<127	908	3275	117
2070-1 457	457	74.7	0.7	0.4	0.5	0.2	<127	583	2069	78
2070-1 463	463	73.5	0.8	0.5	0.5	0.2	<127	475	1619	61
2070-1 467	467	74.9	0.6	0.3	0.5	0.1	<127	321	1149	48
2070-1 471	471	75.5	0.5	0.4	0.5	0.1	<127	425	1452	59
2070-1 472P	472	92.3	0.4	0.2	0.1	<0.09	<127	324	1044	34
2070-1 475	475	74.4	0.8	0.6	0.6	0.3	<127	514	1714	71
2070-1 479	479	72.4	0.9	0.5	0.8	0.3	<127	438	1454	63
2070-1 483	483	73.3	1.0	0.5	0.7	0.2	<127	419	1449	64
2070-1 487	487	76.2	0.7	0.3	0.6	0.2	<127	279	923	44
2070-1 493	493	74.0	2.5	1.4	0.8	0.3	<127	945	3464	107
2070-1 498	498	73.5	2.9	1.8	0.9	0.3	<127	1196	4356	127
2070-1 503	503	72.7	2.9	1.9	0.9	0.4	<127	1045	3891	133
2070-1 508	508	71.2	3.1	2.0	1.0	0.4	<127	852	3126	112
2070-1 513	513	68.0	2.9	1.7	1.0	0.4	<127	976	3543	154
2070-1 517	517	71.9	4.7	3.0	1.1	0.6	<127	1508	5514	187
2070-1 527	527	71.3	5.0	3.4	1.0	0.5	998	2173	8082	236
2070-1 564	564	73.2	1.9	1.2	0.7	0.3	<127	757	2567	92
2070-1 613	613	71.6	2.8	1.8	0.9	0.4	226	1134	4212	138

The quantification limits were determined taking sample dilution factors and lowest concentration of the calibration standards into account

Table S.6: Solution MC-ICP-MS measurements of the silicon isotope composition of reference materials obtained during this study. Individual measurements from different analytical sessions are listed. Average δ-values and their 95% confidence interval (= t·SD/√n), are calculated (intermediate precision of the mass spectrometric method (instrument repeatability). The overall uncertainty of the solution MC-ICP-MS method is estimated to be ± 0.07‰ (2SD) for δ^{29}Si and ± 0.10‰ (2SD) for δ^{30}Si. Averages (± 1SD) of published values (Jochum et al., 2005) of reference materials measured relative to NIST8546 (aka. NBS-28) are as follows. Big Batch: -5.38 ± 0.08‰ δ^{29}Si (n= 8), -10.53 ± 0.19‰ δ^{30}Si (n= 12); IRMM-017: -0.69 ± 0.04‰ δ^{29}Si (n= 3), -1.33 ± 0.08‰ δ^{30}Si (n= 3); BHVO-2: -0.14 ± 0.04‰ δ^{29}Si (n= 12), -0.28 ± 0.05‰ δ^{30}Si (n= 17); Diatomite: 0.64 ± 0.02‰ δ^{29}Si (n= 9), 1.24 ± 0.06‰ δ^{30}Si (n= 15).

Big Batch	**δ^{29}Si [‰]**	**δ^{30}Si [‰]**	**date**
029-BigBatch	-5.41	-10.62	24.05.2012
039-BigBatch	-5.48	-10.68	24.05.2012
029-BigBatch	-5.47	-10.71	05.06.2012
065-BigBatch	-5.43	-10.72	05.06.2012
033-BigBatch	-5.44	-10.66	18.06.2012
063-BigBatch	-5.46	-10.70	18.06.2012
093-BigBatch	-5.50	-10.81	18.06.2012
033-BigBatch	-5.43	-10.68	30.07.2012
063-BigBatch	-5.44	-10.66	30.07.2012
017-BigBatch	-5.41	-10.64	30.07.2012
037-BigBatch	-5.41	-10.60	19.06.2012
073-BigBatch	-5.42	-10.67	19.06.2012
003-BigBatch	-5.42	-10.61	19.11.2012
059-BigBatch	-5.49	-10.76	19.11.2012
003-BigBatch	-5.48	-10.75	06.05.2013
085-BigBatch	-5.44	-10.74	06.05.2013
143-BigBatch	-5.44	-10.69	06.05.2013
187-BigBatch	-5.43	-10.67	06.05.2013
average	**-5.45**	**-10.69**	
95%CI	0.01	0.03	
2SD	0.06	0.11	

IRMM-017	**δ^{29}Si [‰]**	**δ^{30}Si [‰]**	**date**
009-IRMM17	-0.72	-1.43	24.05.2012
039-IRMM17	-0.66	-1.31	24.05.2012
069-IRMM17	-0.65	-1.30	24.05.2012
099-IRMM17	-0.70	-1.30	24.05.2012
033-IRMM17	-0.66	-1.36	24.05.2012
041-IRMM17	-0.59	-1.25	24.05.2012
009-IRMM17	-0.72	-1.43	05.06.2012
039-IRMM17	-0.66	-1.31	05.06.2012
069-IRMM17	-0.65	-1.30	05.06.2012
099-IRMM17	-0.70	-1.30	05.06.2012
007-IRMM17	-0.71	-1.38	06.05.2013
091-IRMM17	-0.73	-1.33	06.05.2013
149-IRMM17	-0.69	-1.41	06.05.2013
191-IRMM17	-0.70	-1.39	06.05.2013
average	**-0.68**	**-1.34**	
95%CI	0.02	0.03	
2SD	0.07	0.11	

BHVO-2	**δ^{29}Si**	**δ^{30}Si**	**date**
039-BHVO	-0.15	-0.29	24.05.2012
005-BHVO	-0.21	-0.36	18.06.2012
035-BHVO	-0.15	-0.28	18.06.2012
065-BHVO	-0.13	-0.27	18.06.2012
095-BHVO	-0.19	-0.38	18.06.2012
005-BHVO	-0.12	-0.25	19.11.2012
061-BHVO	-0.11	-0.25	19.11.2012
average	**-0.15**	**-0.30**	
95%CI	0.03	0.05	
2SD	0.07	0.11	

Diatomite	**δ^{29}Si**	**δ^{30}Si**	**date**
043-Diatomite	0.66	1.23	19.11.2012
077-Diatomite	0.64	1.19	19.11.2012
007-Diatomite	0.63	1.25	30.07.2012
037-Diatomite	0.64	1.24	30.07.2012
067-Diatomite	0.61	1.23	30.07.2012
021-Diatomite	0.66	1.28	30.07.2012
005-Diatomite	0.62	1.27	06.05.2013
087-Diatomite	0.63	1.26	06.05.2013
147-Diatomite	0.65	1.22	06.05.2013
189-Diatomite	0.63	1.19	06.05.2013
059-Diatomite	0.64	1.27	31.02.2013
119-Diatomite	0.63	1.23	31.02.2013
123-Diatomite	0.65	1.27	31.02.2013
average	**0.64**	**1.24**	
95%CI	0.01	0.02	
2SD	0.03	0.06	

Table S.6 cont.

Herasil	$\delta^{29}Si$	$\delta^{30}Si$	date
035-Herasil	-0.06	-0.14	24.05.2012
007-Herasil	-0.09	-0.16	18.06.2012
037-Herasil	-0.03	-0.17	18.06.2012
067-Herasil	-0.03	-0.07	18.06.2012
097-Herasil	-0.10	-0.19	18.06.2012
039-Herasil	-0.08	-0.22	19.06.2012
075-Herasil	-0.06	-0.17	19.06.2012
005-Herasil	-0.08	-0.13	30.07.2012
035-Herasil	-0.05	-0.18	30.07.2012
065-Herasil	0.00	-0.04	30.07.2012
019-Herasil	-0.04	-0.05	30.07.2012
011-Herasil	-0.08	-0.13	06.05.2013
093-Herasil	-0.11	-0.19	06.05.2013
151-Herasil	-0.10	-0.12	06.05.2013
195-Herasil	-0.03	-0.11	06.05.2013
average	**-0.06**	**-0.14**	
95%CI	0.02	0.03	
2SD	0.06	0.10	

Table S.7: fs-laser ablation MC-ICP-MS measurements of the silicon isotope composition of reference materials obtained during this study. The internal standard error of the mean (2SE) is given for each single sample measurements (comprising n= 80 integrations á 1 second for sample and 2 bracketing standards). The uncertainty of the fsLA-MC-ICP-MS method (external long-term repeatability) is ± 0.15‰ (2SD) for δ^{29}Si and ± 0.23‰ (2SD) for δ^{30}Si, respectively. Averages (±1SD) of published values (Jochum et al., 2005) of reference materials measured relative to NIST8546 (aka. NBS-28) are as follows. IRMM-017: -0.69 ± 0.04‰ δ^{29}Si (n= 3), -1.33 ± 0.08‰ δ^{30}Si (n= 3); BHVO-2: -0.14 ± 0.04‰ δ^{29}Si (n= 12), -0.28 ± 0.05‰ δ^{30}Si (n= 17).

BHVO-2G	**δ^{29}Si [‰]**	**2SE**	**δ^{30}Si [‰]**	**2SE**	**date**
003-BHVO_1	-0.12	0.12	-0.29	0.23	03.08.2012
015-BHVO_2	-0.21	0.14	-0.40	0.26	03.08.2012
035-BHVO_3	-0.09	0.14	-0.34	0.26	03.08.2012
055-BHVO_4	-0.15	0.15	-0.35	0.24	03.08.2012
075-BHVO_5	-0.31	0.18	-0.63	0.35	03.08.2012
average	**-0.18**		**-0.40**		
95%CI	0.10		0.16		
005-BHVO1	-0.25	0.16	-0.63	0.23	01.08.2012
029-BHVO2	-0.11	0.07	-0.36	0.11	01.08.2012
053-BHVO3	-0.16	0.08	-0.46	0.12	01.08.2012
077-BHVO4	-0.20	0.08	-0.30	0.11	01.08.2012
101-BHVO5	-0.16	0.10	-0.18	0.13	01.08.2012
125-BHVO6	-0.18	0.09	-0.25	0.13	01.08.2012
131-BHVO7	-0.20	0.10	-0.26	0.14	01.08.2012
average	**-0.18**		**-0.35**		
95%CI	0.04		0.14		

BHVO-2G	**δ^{29}Si**	**2SE**	**δ^{30}Si**		**date**
011-BHVO	-0.09	0.07	-0.17	0.11	11.02.2013
013-BHVO	-0.06	0.08	-0.11	0.12	11.02.2013
015-BHVO	-0.04	0.07	-0.08	0.11	11.02.2013
057-BHVO	-0.01	0.08	-0.02	0.11	11.02.2013
059-BHVO	-0.06	0.08	-0.12	0.12	11.02.2013
061-BHVO	-0.04	0.08	-0.08	0.11	11.02.2013
103-BHVO	-0.09	0.07	-0.18	0.10	11.02.2013
105-BHVO	-0.09	0.08	-0.19	0.12	11.02.2013
107-BHVO	-0.02	0.07	-0.04	0.11	11.02.2013
149-BHVO	-0.17	0.08	-0.33	0.11	11.02.2013
151-BHVO	-0.14	0.08	-0.27	0.12	11.02.2013
153-BHVO	-0.09	0.08	-0.17	0.11	11.02.2013
189-BHVO	-0.07	0.08	-0.14	0.12	11.02.2013
191-BHVO	0.02	0.08	0.04	0.12	11.02.2013
average	**-0.07**		**-0.13**		
95%CI	0.03		0.06		

all BHVO-2G data

average	**-0.12**		**-0.24**
2SD	**0.15**		**0.34**
95%CI	0.03		0.07

Table S.7 cont.

IRMM-017	**$\delta^{29}Si$**	**2SE**	**$\delta^{30}Si$**	**2SE**	**date**
005-IRMM17_1	-0.67	0.07	-1.35	0.11	8/3/2012
025-IRMM17_2	-0.66	0.08	-1.20	0.12	8/3/2012
045-IRMM17_3	-0.65	0.07	-1.32	0.11	8/3/2012
065-IRMM17_4	-0.64	0.10	-1.34	0.13	8/3/2012
087-IRMM17_5	-0.75	0.08	-1.36	0.12	8/3/2012
average	**-0.67**		**-1.31**		
95%CI	0.05		0.08		
129-IRMM17	-0.61	0.11	-1.00	0.17	8/1/2012
017-IRMM17_2	-0.58	0.10	-1.15	0.16	8/1/2012
041-IRMM17_3	-0.64	0.09	-1.13	0.13	8/1/2012
065-IRMM17_4	-0.59	0.11	-1.26	0.13	8/1/2012
089-IRMM17_5	-0.55	0.12	-1.08	0.16	8/1/2012
average	**-0.59**		**-1.12**		
95%CI	0.04		0.11		

IRMM-017	**$\delta^{29}Si$**	**2SE**	**$\delta^{30}Si$**		**date**
003-IRMM17	-0.71	0.08	-1.39	0.12	2/11/2013
005-IRMM17	-0.71	0.08	-1.39	0.12	2/11/2013
007-IRMM17	-0.69	0.07	-1.35	0.11	2/11/2013
009-IRMM17	-0.68	0.09	-1.34	0.14	2/11/2013
193-IRMM17	-0.67	0.08	-1.31	0.11	2/11/2013
195-IRMM17	-0.69	0.07	-1.35	0.11	2/11/2013
197-IRMM17	-0.76	0.08	-1.50	0.12	2/11/2013
average	**-0.70**		**-1.37**		
95%CI	0.03		0.05		

all IRMM-017 data			
average	**-0.66**		**-1.28**
2SD	**0.11**		**0.26**
95%CI	0.03		0.07

Leaching experiments on siliceous sediments

Table S.8: Experimental conditions for leaching experiments.

Experiment #	I (sequential extraction)	II (batch extraction)
Sample	PS2070-1-423	IIa: PS2070-1-493 IIb: PS2089-2-639
Sample mass [mg]	5.3	2.6 - 3
Vol. 1.6 mM NaOH [ml]	50	25
increased to 1M NaOH	after 5 hours	-
	1 aliquot of sample powder with continuous sampling from one tube	12 separate sample powder aliquots (+NaOH) sampled once after given time
T [°C]	≈ 70°C	20°C after 0.5, 1, 1.5, 2, 2.5, 3, 3.5, 4, 5, 6, 8 and 22.5 h; 70°C after 24 h
Mixing	occasional shaking by hand	roller mixer for leaching experiment IIa at 20°C in PP tubes; exp. IIb convection in Teflon vials on hot plate for leaching experiments at 70°C
Sampling interval	every 30 min for 5h, then after 6.5h, 22.5h, respectively	every 30 to 60 min for 5h, then after 6h, 8h, 22.5h, 24h, respectively

Table S.9: Solution MC-ICP-MS silicon isotope data of solutions sampled during leaching of siliceous sediments in NaOH. Leaching experiment I (on sample PS2070-1-423) was conducted using one solution that was repeatedly sampled. In experiments IIa (PS2070 1-493) and IIb (PS2089-2-639) twelve separate tubes were sampled separately. See main text and table S.8 for details. Samples V123a and V456a represent mixtures of samples with too low Si amounts for individual Si isotope analyses. Average δ-values of n replicate measurements and their 95% confidence intervals (= t·SD/√n) are reported. 95%CI indicates the intermediate precision of the mass spectrometric method (instrument repeatability). The overall uncertainty of the solution MC-ICP-MS method is estimated to be ± 0.07‰ (2SD) for δ^{29}Si and ± 0.10‰ (2SD) for δ^{30}Si, which should be used for data interpretation (also for analysis results with n= 1). Uncertainty in Al and Si concentration data measured by ICP-OES are estimated to be 5% relative.

sample	time [h]	T [°C]	NaOH [mM]	δ^{29}Si [‰]	95%CI	δ^{30}Si [‰]	95%CI	n	Al [ppm]	Si [ppm]	Al/Si
leaching experiment I (single aliquot extraction; sample PS2070-1-423)											
V123a	0.5 - 1.5	70	1.6	0.41	0.04	0.75	0.08	4	0.94	6.2	0.15
V456a	2 - 3	70	1.6	0.73	0.05	1.45	0.12	3	1.55	17.1	0.09
V7a	3.5	70	1.6	0.73	0.01	1.42	0.05	3	0.80	9.6	0.08
V8a	4	70	1.6	0.74	0.03	1.40	0.09	3	2.76	34.1	0.08
V9a	4.5	70	1.6	0.66	0.10	1.35	0.15	3	1.41	16.3	0.09
V10a	5	70	1.6	0.62	0.03	1.23	0.05	3	0.27	7.1	0.04
V12a	6.5	70	1000	0.45	0.02	0.88	0.12	3	0.07	18.1	0.00
V13a	22.5	70	1000	0.13	0.06	0.29	0.07	4	0.30	61.7	0.00
leaching experiment IIa (multiple aliquot extraction; sample PS2070-1-493)											
493_1	0.5	20	1.6	0.40		0.55		1	0.15	2.2	0.07
493_4	2	20	1.6	0.38		0.64		1	0.10	1.7	0.06
493_5	2.5	20	1.6	0.39		0.62		1	0.11	2.1	0.05
493_6	3	20	1.6	0.41		0.66		1	0.05	1.4	0.04
493_7	3.5	20	1.6	0.41	0.09	0.71	0.04	3	0.10	3.2	0.03
493_8	4	20	1.6	0.42	0.15	0.73	0.56	2	0.03	1.2	0.02
493_9	5	20	1.6	0.38	0.38	0.67	0.60	2	0.22	4.0	0.05
493_10	6	20	1.6	0.32	0.14	0.57	0.30	2	0.09	1.8	0.05
493_11	8	20	1.6	0.45	0.03	0.74	0.08	3	0.11	2.9	0.04
493_12	22.5	20	1.6	0.58	0.09	1.08	0.07	4	0.37	4.1	0.09
493_13	24	70	1.6	0.33	0.05	0.68	0.04	4	0.10	16.5	0.01
leaching experiment IIb (multiple aliquot extraction; PS2070-1-639)											
693_1	0.5	20	1.6	0.26		0.28		1	0.05	2.0	0.02
693_2	1	20	1.6	0.17		0.38		1	0.07	2.3	0.03
693_5	2.5	20	1.6	0.18		0.32		1	0.05	1.1	0.04
693_6	3	20	1.6	0.23		0.43		1	0.04	1.2	0.03
693_7	3.5	20	1.6	0.26	0.14	0.55	0.14	3	0.09	3.9	0.02
693_8	4	20	1.6	0.19	0.27	0.34	0.33	2	0.08	2.0	0.04
693_9	5	20	1.6	0.25		0.41		1	0.05	1.3	0.03
693_10	6	20	1.6	0.23	0.42	0.42	0.63	2	0.04	1.6	0.03
693_11	8	20	1.6	0.29	0.12	0.48	0.41	2	0.05	1.3	0.04
693_12	22.5	20	1.6	0.39	0.07	0.74	0.05	3	0.07	2.0	0.03
693_13	24	70	1.6	0.52	0.02	1.00	0.07	4	0.09	10.5	0.01

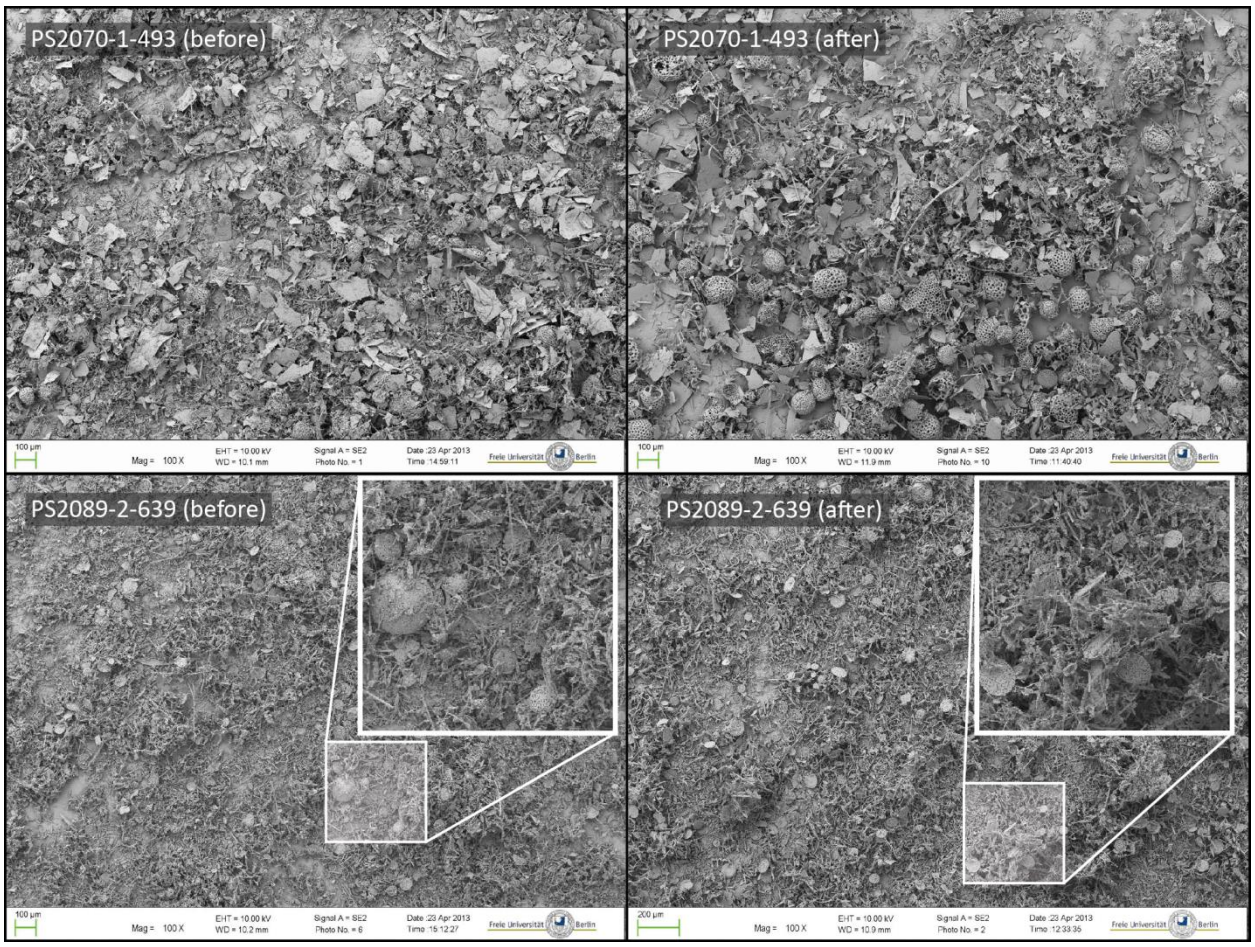

Figure S.1: Secondary electron microscopy (SEM) images obtained before and after the leaching treatment of samples PS2070-1-493 (experiment IIa) and PS2089-2-639 (experiment IIb) with 1.6 mM NaOH for 24 hours at 70°C. A relative increase of radiolarians is apparent in sample PS2070-1-493, after 43% of the total silica has been dissolved. Sample PS2089-2-639 almost exclusively contains diatoms and no obvious changes in composition occur after 27% of the total silicon has been dissolved.

Supplementary References

Cardinal, D., Alleman, L.Y., de Jong, J., Ziegler, K., André, L., 2003. Isotopic composition of silicon measured by multicollector plasma source mass spectrometry in dry plasma mode. J. Anal. At. Spectrom. 18, 213–218. doi:10.1039/b210109b

Chmeleff, J., Horn, I., Steinhoefel, G., von Blanckenburg, F., 2008. In situ determination of precise stable Si isotope ratios by UV-femtosecond laser ablation high-resolution multi-collector ICP-MS. Chem. Geol. 249, 155–166. doi:10.1016/j.chemgeo.2007.12.003

Jochum, K.P., Nohl, U., Herwig, K., Lammel, E., Stoll, B., Hofmann, A.W., 2005. GeoReM: A New Geochemical Database for Reference Materials and Isotopic Standards. Geostand. Geoanalytical Res. 29, 333–338. doi:10.1111/j.1751-908X.2005.tb00904.x

Reynolds, B.C., Aggarwal, J., André, L., Baxter, D., Beucher, C., Brzezinski, M. a., Engström, E., Georg, R.B., Land, M., Leng, M.J., Opfergelt, S., Rodushkin, I., Sloane, H.J., van den Boorn, S.H.J.M., Vroon, P.Z., Cardinal, D., 2007. An inter-laboratory comparison of Si isotope reference materials. J. Anal. At. Spectrom. 22, 561–568. doi:10.1039/b616755a

Savage, P.S., Armytage, R.M.G., Georg, R.B., Halliday, A.N., 2014. High temperature silicon isotope geochemistry. Lithos 190-191, 500–519. doi:10.1016/j.lithos.2014.01.003

Schoenberg, R., von Blanckenburg, F., 2005. An assessment of the accuracy of stable Fe isotope ratio measurements on samples with organic and inorganic matrices by high-resolution multicollector ICP-MS. Int. J. Mass Spectrom. 242, 257–272. doi:10.1016/j.ijms.2004.11.025

Schuessler, J.A., von Blanckenburg, F., 2014. Testing the limits of micro-scale analyses of Si stable isotopes by femtosecond laser ablation multicollector inductively coupled plasma mass spectrometry with application to rock weathering. Spectrochim. Acta Part B At. Spectrosc. 98, 1–18. doi:10.1016/j.sab.2014.05.002